Bayesian Fault Detection and Localization Through Wireless Sensor Networks in Industrial Plants

Gianluca Tabella, *Graduate Student Member, IEEE,* Domenico Ciuonzo, *Senior Member, IEEE,*
Nicola Paltrinieri, and Pierluigi Salvo Rossi, *Senior Member, IEEE*

Abstract—This work proposes a data fusion approach for quickest fault detection and localization within industrial plants via wireless sensor networks. Two approaches are proposed, each exploiting different network architectures. In the first approach, multiple sensors monitor a plant section and individually report their local decisions to a fusion center. The fusion center provides a global decision after spatial aggregation of the local decisions. A post-processing center subsequently processes these global decisions in time, which performs quick detection and localization. Alternatively, the fusion center directly performs a spatio-temporal aggregation directed at quickest detection, together with a possible estimation of the faulty item. Both architectures are provided with a feedback system where the network's highest hierarchical level transmits parameters to the lower levels. The two proposed approaches model the faults according to a Bayesian criterion and exploit the knowledge of the reliability model of the plant under monitoring. Moreover, adaptations of the well-known Shewhart and CUSUM charts are provided to fit the different architectures and are used for comparison purposes. Finally, the algorithms are tested via simulation on an active Oil and Gas subsea production system, and performances are provided.

Index Terms—Data fusion, fault detection, Industry 4.0, localization, monitoring, quickest detection, reliability, wireless sensor network.

I. INTRODUCTION

OVER the last decades, Wireless Sensor Networks (WSNs) have surged in growth, harnessing low-cost "green" devices for monitoring applications [2]. Fueled by the advances in sensor technology, wireless communication protocols, and the popularization of the Internet of Things (IoT) [3], this expansion has ushered in a new era of data acquisition and situation awareness. WSNs, as the sensing arm of the IoT, play a pivotal role in this paradigm, seamlessly merging the physical and digital realms through real-time data for diverse inference tasks [4].

Specifically, there has been a considerable focus on the detection and localization of adverse events, with a particular emphasis on their application in developing safeguards for safety-critical systems. This situation holds considerable importance in sectors like the process industry, energy production, and manufacturing, where the malfunction of a single component (the event under scrutiny) could jeopardize the well-being of both employees and the environment. Consequently, this could lead to significant environmental and societal expenses, as well as substantial financial losses resulting from unexpected shutdowns [5]. For that reason, the global critical infrastructure protection market currently commands a valuation of USD 132 billion, and forecasts indicate a steady 3.4% compound annual growth rate through 2030. In this context, IoT technologies will play a dominant role [6]. In light of those reasons, the exploration of event detection using Wireless Sensor Networks (WSNs) for industrial purposes has garnered significant attention. Various architectural designs have been scrutinized and put forth, with a specific focus on underwater applications, as referenced in previous literature [7], [8].

A pivotal concern in this context revolves around identifying equipment malfunctions that could potentially result in *loss of containment*. This concern is particularly pronounced in settings where inspections come at a substantial cost, such as subsea facilities, as indicated by prior research [9], [10].

On top of that, to lower communication and processing costs (thus prolonging the WSN lifetime and reducing monitoring costs), the sensors are typically engineered to communicate 1-bit decisions to a Fusion Center (FC), which gathers such decisions and formulates a global decision regarding the presence of the event of interest (in our case a fault on the monitored plant) [11], [12]. Upon detecting a hostile event, the FC generates an alarm, enabling appropriate measures (e.g., emergency plant maintenance) to be implemented in order to mitigate the event's repercussions.

It is important to highlight that the efficacy of a system for detecting and localizing faults also depends on how well it is integrated into a risk management framework. This integration allows full exploitation of the amount of information available about the surveilled system during the design stage of the fault detection and localization system. A suitable integration can be achieved by using the *Dynamic Risk Management Framework* (DRMF), which is designed to incorporate external experiences and early warnings, thereby allowing the assimilation of unknown variables [13]–[16]. Enhanced risk awareness associated with unforeseen events enables learning and understanding, which is based on the continuous *monitoring* and *review* of

accumulated information. DRMF involves several steps, such as (i) *horizon screening*, (ii) *hazard identification*, (iii) *assessment*, and finally (iv) *decision/action*. These steps are necessary for a comprehensive evaluation of the risks connected to known potential accident scenarios. To make the DRMF an adaptive process, iterative updates are essential. In this context, the fault detection and localization system serves as a warning subsystem within a decision-support system by playing a role in actions like plant shutdown and maintenance.

In this context, **peculiar characteristics and challenges for the problem** are: (i) the finite spatial extent of the event being monitored (i.e., some sensors may be out-of-range for detecting a certain fault), (ii) the fault location is unknown (viz. it may have originated from different items of interest within the plant), (iii) each fault may be more or less probable depending on the reliability of the item responsible for it, (iv) efficient detection algorithms should be conceived to detect such events as quickly as possible (viz. minimize the permanence in a risky condition) while keeping false-alarms under control (viz. avoid unnecessary maintenance/shutdowns), (v) detection approaches should be coupled with (or better, include) localization procedures to identify the faulty item (viz. minimize the plant maintenance time/costs).

In the context of challenges (i) and (ii), various algorithms have been proposed in the literature for detecting spatially localized events at unknown locations (such as radiation releases, anomalous parameter fields, or non-cooperative targets) via distributed WSNs. Initial attempts involve the straightforward application [17], [18] or adaptations/extensions [19] (e.g., by using ordering schemes according to most informative sensors) of the sub-optimal *Counting Rule* (CR). Notably, the plain CR has recently found application in the specific domain of subsea oil spill detection [20], [21]. An alternative approach is explored in [10], [22], where a modified version of the *Chair-Varshney Rule* is devised. This rule is designed to partially incorporate critical items' locations and failure rates. Additionally, it is coupled with localization techniques to address challenge (v). Regrettably, these rules do not take into account the *limited extent* and *unknown location* of the detected phenomenon by design. This results in *diminished detection performance*.

Conversely, recent years have witnessed the emergence of a range of fusion rules designed for the explicit detection of spatially localized events with unknown locations through distributed WSNs [12], [23], [24]. To tackle this challenge, these approaches have harnessed methodologies such as the Generalized Likelihood Ratio Test (GLRT), Bayesian techniques, generalized score tests, or hybrid variations. While *primarily focused on detecting non-cooperative targets*, these algorithms can be adapted to address challenges (i), (ii), and (v). However, it is essential to note that the fusion methods mentioned are fundamentally designed in a batch fashion (or overlook temporal dependencies) and fail to target the rapid onset of faults, thus not fully addressing challenge (iv). Recent advancements in this domain have made strides in mitigating the constraints associated with batch design [25], [26]. Nevertheless, these proposals are not able to promptly detect events as they occur, which is crucial in addressing the quickest detection problem.

Furthermore, to the best of our understanding, *no approach has effectively integrated data regarding the dependability of the system being monitored when developing the detection algorithm*, i.e., challenge (iii). Vital data, encompassing the positions, failure rates, and failure models of critical items, represent valuable a-priori information that may be seamlessly substantiated within a Bayesian approach. Hence, the **main contributions** of this work are the following:

- We present two spatio-temporal sensor fusion approaches designed to carry out quickest *detection and localization* of faults within a system. To elaborate, a WSN collectively observes the status of various equipment components and communicates their decisions to *two different classes of architectures*.
- The first architecture (aligning to an edge-fog-cloud paradigm [27]) is composed of a FC which performs *spatial aggregation* and an optimal per-sample decision. These decisions are subsequently processed *over time* by a Post-Processing Center (PPC). The PPC is responsible for swiftly identifying system faults based on a Bayesian approach and takes advantage of time-varying statistical distributions influenced by the reliability data of system components. Differently, the second architecture (aligning to an edge-cloud paradigm) is composed of a FC only, which performs a joint spatio-temporal aggregation in a Bayesian quickest detection fashion. These architectures are compared with baselines represented by the Shewhart and CUSUM charts, respectively, as well as in terms of their computational complexity.
- The outcomes of the suggested methods are examined with a specific focus on a practical Oil and Gas configuration, specifically the subsea production system of the Goliat FPSO [28]. The results, encompassing both (i) detection and localization as well as (ii) metrics emphasizing reliability, underscore the attractiveness of the proposed methods and the added advantage of temporal aggregation compared to relying solely on spatial aggregation.

This study delves deeper into the application of WSNs for fault detection and localization, incorporating reliability-related item data into the same detection algorithm(s) as previously introduced in [1]. Indeed, this earlier conference work: (i) analyzed a Three-Layer architecture; (ii) provided a comparison with a Shewhart chart; (iii) reported a preliminary numerical analysis using only one threshold value; (v) focused on the detection task without providing a localization algorithm. Conversely, this work investigates and compares two relevant fusion architectures (i.e., two- vs. three-layer) to accommodate a larger spectrum of designer requirements using a wide number of detection thresholds. Secondly, additional baselines are included in the comparison (i.e., the CUSUM chart). Thirdly, the proposed design includes fault-localization capabilities.

The paper's remaining sections are arranged as follows. Sec. II provides a description of the system model considered (including failure and corresponding sensing models), whereas Sec. III presents the design of the local detectors that is common to all the architectures discussed in this work. Then, Sec. IV recalls the state-of-the-art in industrial fault identification,

whereas Secs. V and VI are devoted to introducing the considered Three-Layer and Two-Layer fusion approaches, respectively. Sec. VIII analyzes the proposed approaches' pros and cons in relation to a relevant case study concerning oil spills in a production platform and discusses the results. Finally, Sec. IX ends the paper with concluding remarks and a brief prospect of future avenues of research.

Notation – vectors are indicated with bold letters; the norm and transpose operators are represented as $\| \cdot \|$ and $[\cdot]^{\mathrm{T}}$; probability mass functions (PMFs) and probability density functions (PDFs) are denoted as $\mathbb{P}(\cdot)$ and $p(\cdot)$, respectively; conditional counterparts are represented by $\mathbb{P}(\cdot|\cdot)$ and $p(\cdot|\cdot)$; a Gaussian distribution with mean μ and variance σ^2 is labeled as $\mathcal{N}(\mu, \sigma^2)$; the complementary cumulative distribution function (CCDF) of the standard normal distribution is denoted by $\mathcal{Q}(\cdot)$; an exponential distribution with rate λ is expressed as $\mathrm{Exp}(\lambda)$; a Bernoulli distribution with parameter p is symbolized as $\mathcal{B}(p)$; a Gamma distribution with shape α and rate β is indicated by $\mathrm{Gamma}(\alpha, \beta)$; a Poisson distribution with parameter p is represented as $\mathrm{Poisson}(p)$; $G_a(z)$ expresses the probability-generating function of the discrete random variable a; $a^+ \triangleq \max\{a, 0\}$ defines the positive component of the real number a; $\widehat{a}$, $\mathbb{E}(a)$, and $\mathbb{E}(a|b)$ stand for an estimate of the random variable a, its expected value, and conditional expectation given the random variable b, respectively; the big O notation is denoted by $\mathcal{O}(\cdot)$.

II. SYSTEM MODEL

This work has the objective of *detecting* and *localizing* faults within a given set of critical items associated with an industrial plant (e.g., the subsea production system of an offshore oil platform). The failure model associated with each of these items is described and motivated in Sec. II-A. Possible faults are monitored by a group of inexpensive sensor nodes (arranged in a WSN), whose measurement model is detailed in Sec. II-B. At each instant, the sensor computes a one-bit compression based on a local detection logic, which is then reported for (time and spatial) aggregation according to the considered fusion architectures, as described in Sec. II-C.

A. Failure Model

The monitored portion of the plant is conceptualized as a system comprising M individual *items*. Each item's state at time t is represented by the following variable:

$$\mathcal{H}_m(t) = \begin{cases} 0, & m\text{th item is } \textbf{operational} \\ 1, & m\text{th item is } \textbf{faulty} \end{cases}, \quad (1)$$

where *operational* indicates that the item is functioning as intended with no immediate action required, while *faulty* signifies that the item needs maintenance. Moreover, we define the state variable at time t for the *whole system* as:

$$\mathcal{H}(t) = 1 - \prod_{m=1}^{M} (1 - \mathcal{H}_m(t)) = \begin{cases} 0, & \textbf{operational} \text{ system} \\ 1, & \textbf{faulty} \text{ system} \end{cases}, \quad (2)$$

implying *independent failures and that the system is regarded as faulty when at least one of its items is in such state (i.e.,*
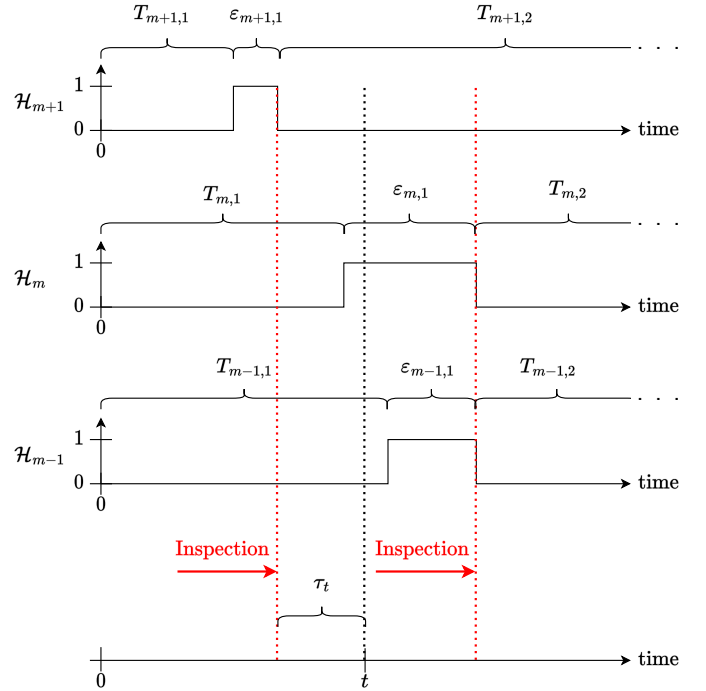

Fig. 1: Failure model (excluding inspection and maintenance durations).

series system). An item retains a faulty state until maintenance is carried out. In the present work, we assume that, when an item becomes faulty, the sensors employed to monitor the system measure a signal with a different statistical distribution. Upon identifying a shift in the signal distribution, an inspection is carried out to evaluate the overall state of the system, and maintenance is subsequently executed on all items that have malfunctioned.

The occurrence of a failure in the mth item is represented as a *homogeneous Poisson process* characterized by a *failure rate* λ_m (refer to Fig. 1).

Let us define $T_{m,j}$ as the amount of time the mth item spends in an operational state between the $(j-1)$th and the jth failures and $\mathcal{S}_m(t)$ as the number of transitions to a faulty state for the mth item at time t. It follows that $T_{m,j} \sim \mathrm{Exp}(\lambda_m)$ for all $j \in \mathbb{N}$. Furthermore, we introduce $T_{m,j}^* \triangleq T_{m,j} + \varepsilon_{m,j}$, where $\varepsilon_{m,j}$ represents the time elapsed before the failure state is detected. At time t, we define τ_t as the time elapsed since the most recent inspection. Because Poisson processes are *memoryless*, maintenance can be considered as either repair or replacement. A consequence of the failure model is the derivation of the *failure function* (or *failure probability*) for the mth item, as expressed by Eq. (3):

$$F_m(t) \triangleq \mathbb{P}(\mathcal{H}_m(t) = 1) = 1 - e^{-\lambda_m \tau_t}. \quad (3)$$

Subsequently, the failure function for the entire system at a given time t is determined by Eq. (4):

$$F(t) \triangleq \mathbb{P}(\mathcal{H}(t) = 1) = 1 - \prod_{m=1}^{M} (1 - F_m(t)). \quad (4)$$

This expression of $F(t)$ indicates independent failures. Moreover, for sufficiently small values of $\lambda_m \tau_t$ (i.e., $\lambda_m \tau_t \ll 1$), we simplify the model as:

$$F(t) \approx \sum_{m=1}^{M} F_m(t) = M - \sum_{m=1}^{M} e^{-\lambda_m \tau_t} . \qquad (5)$$

Such approximation (henceforth called *rare events approximation*) is widely used when the items forming the monitored system have sufficiently low values of $F_m(t)$'s resulting in their products becoming negligible [29].

Furthermore, according to Eq. (5), it suggests the occurrence of *disjoint failures*. This implies that at any given time t, *at most one item will be faulty*, a characteristic that will be considered in the detectors' design. The rare event approximation allows us to define a *prior probability of item failure* for the mth item labeled as $\varphi_m(t)$:

$$\varphi_m(t) \triangleq \mathbb{P}(\mathcal{H}_m(t) = 1|\mathcal{H}(t) = 1) \approx \frac{\mathbb{P}(\mathcal{H}_m(t) = 1)}{\mathbb{P}(\mathcal{H}(t) = 1)}$$
$$= \frac{F_m(t)}{F(t)} = \frac{1 - e^{-\lambda_m \tau_t}}{M - \sum\limits_{m=1}^{M} e^{-\lambda_m \tau_t}} . \qquad (6)$$

Such a probability can also be expressed in a time-independent fashion. In such case, we can define a *stationary prior probability of item failure* for the mth φ_m:

$$\varphi_m \triangleq \frac{\lambda_m}{\sum\limits_{m=1}^{M} \lambda_m} . \qquad (7)$$

A detailed treatment of the mathematical modeling of the failures as Poisson processes is given in Appendix A.

Throughout the paper, the system monitoring occurs at regular time intervals of duration Δt, with the exception of inspection and maintenance periods. Therefore, in order to ease the readability of this work, we consider the nth discrete time instant, with n_0 indicating the first discrete time instant that follows the last inspection.

B. Signal Model

The expression for the received signal $y_k[n]$ at the kth sensor during the nth discrete time point is as follows:

$$y_k[n] = \sum_{m=1}^{M} s_{m,k}[n] + w_k[n] , \qquad (8)$$

where $s_{m,k}[n]$ and $w_k[n] \sim \mathcal{N}(0, \sigma_{w,k}^2)$ represent the received signal from the mth item and the Additive White Gaussian Noise (AWGN), respectively, at the kth sensor. More specifically, $s_{m,k}[n]$ is assumed to have the following shape:

$$s_{m,k}[n] \triangleq \begin{cases} 0, & \text{if } \mathcal{H}_m[n] = 0 \text{ (active item)} \\ \xi_{m,k}[n]\, g(\boldsymbol{x}_k, \boldsymbol{h}_m), & \text{if } \mathcal{H}_m[n] = 1 \text{ (faulty item)} \end{cases}, \qquad (9)$$

where $\xi_{m,k}[n] \sim \mathcal{N}(0, \sigma_{\xi,m}^2)$ represents the fluctuations in the received signal strength at the kth sensor. $\xi_{m,k}[n]$ and $w_k[n]$ are assumed statistically independent thanks to the spatial

separation of the sensors with *known* values of $\sigma_{\xi,m}^2$ and $\sigma_{w,k}^2$, for all $k = 1, \ldots, K$ and $m = 1, \ldots, M$. Lastly, $g(\boldsymbol{x}_k, \boldsymbol{\theta}_m)$ denotes the attenuation function, which is a function of the distance between the location of the kth sensor ($\boldsymbol{x}_k$) and the position of the mth item ($\boldsymbol{\theta}_m$).

This model is suitable for several practical industrial settings like the acoustic signal generated by an underwater leak sensed by hydrophones [1], [10].

It is important to note that the rare event approximation introduced in Eq. (5) hinders the possibility of modeling more than one item being faulty at a given time. Thus, for any given time instance denoted as n, we can express the statistical characteristics of the measured signal as follows (see Eq. (10)):

$$\begin{cases} y_k[n]|\mathcal{H}[n] = 0 \sim \mathcal{N}\left(0, \sigma_{w,k}^2\right) \\ y_k[n]|\mathcal{H}_m[n] = 1 \sim \mathcal{N}\left(0, \sigma_{\xi,m}^2\, g^2(\boldsymbol{x}_k, \boldsymbol{\theta}_m) + \sigma_{w,k}^2\right) \end{cases}, \qquad (10)$$

where it is important to state that the failure of the generic mth item caused the system to be faulty.

C. Wireless Sensor Network Models

In this work, we design **two fusion architectures**. The first uses an *edge-fog-cloud* approach where the network can be separated into three hierarchical layers with growing computational power as we approach the cloud layer, as it can be seen in Fig. 2a. In contrast, the second uses two hierarchical layers, i.e., an *edge-cloud approach*, as shown in Fig. 2b. Both architectures are proposed with an integrated feedback system that transmits updated parameters from the cloud layer to the lower layers.

The integration of an *edge-fog-cloud* architecture is particularly justified in scenarios where sensors are required to operate with minimal energy consumption. This need is exemplified in the context of underwater WSN, where the replacement of sensors is impractical, underscoring the critical importance of preserving their battery life (refer to the case study in Sec. VIII). By incorporating an underwater fog layer (FC), energy consumption during data transmission by sensors can be significantly reduced. Subsequently, this fog layer can transmit compressed information to a cloud layer (PPC) for final processing.

The proposed WSN architectures comprise a set of K sensors responsible for monitoring the area of interest at regular intervals of time Δt, aiming to identify if the system is in an operational ($\mathcal{H}[n] = 0$) or a faulty state ($\mathcal{H}[n] = 1$).[1] The generic kth sensor is tasked with capturing and assessing the signal $y_k[n]$. It does so by comparing a statistic derived from the measured signal to a threshold value that varies with time, denoted as $\gamma_k[n]$. Subsequently, the sensor reaches a local decision $d_k[n] = i$ when it declares $\mathcal{H}[n] = i$. Such a decision is then reported for further analytics. The latter choice not only offers spectral efficiency, requiring only 1-bit communication on the reporting channel linking the sensors to the fusion architecture, but it also exhibits high energy

[1]It is important to note that the present work does not delve into the analysis of the sampling frequency.
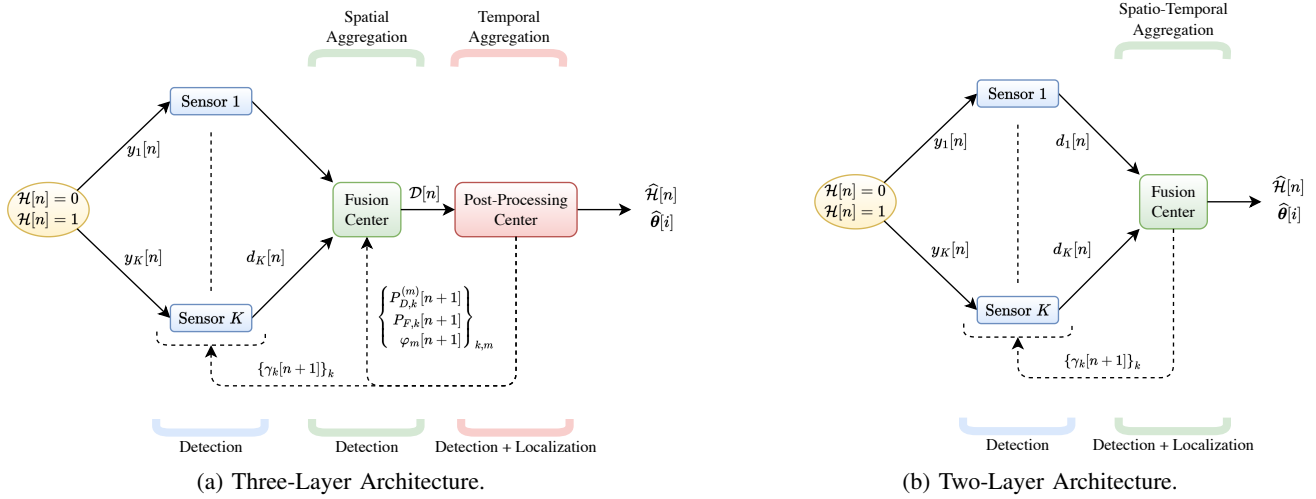
Fig. 2: Proposed Wireless Sensor Network architectures (the dotted arrow constitutes the feedback system).

efficiency, especially when On-Off Keying (OOK) is utilized for transmitting the local decisions (see [10] for more details).

1) Three-Layer Fusion Architecture: The first WSN we propose incorporates an architecture consisting of a *fusion center* (FC) and a *post-processing center* (PPC), performing spatial and temporal aggregation, respectively. In this setup, the vector of local decisions $\boldsymbol{d}[n] = \begin{bmatrix} d_1[n] & \cdots & d_K[n] \end{bmatrix}^{\mathrm{T}}$ is gathered and processed at the FC for a global decision $\mathcal{D}[n] = i$ if $\mathcal{H}[n] = i$ is declared.

The FC performs a *Maximum Likelihood (ML) detection* based on the binary hypothesis as defined in Eq. (10), without assuming prior knowledge about the probabilities of events $\mathcal{H}[n] = 0$ and $\mathcal{H}[n] = 1$. On the other hand, the PPC collects $\boldsymbol{\mathcal{D}}[n] = \begin{bmatrix} \mathcal{D}[n_0] & \cdots & \mathcal{D}[n] \end{bmatrix}^{\mathrm{T}}$ and incorporates information from the failure model as well as the signal model defined in Eqs. (8) and (10). The PPC makes a final decision $\widehat{\mathcal{H}}[n]$ through a *Bayesian posterior detection*, with $\widehat{\mathcal{H}}[n] = 1$ triggering inspection operations.

Moreover, in the case of $\widehat{\mathcal{H}}[n] = 1$, the PPC computes the estimated position of the faulty item $\widehat{\boldsymbol{\theta}}[i] = \boldsymbol{\theta}_{\widehat{m}[i]}$, where i indicates the number of times an alarm has been raised, up to instant n. Additionally, the PPC is responsible for ongoing communication with the sensors, providing them with updated values for their individual time-dependent thresholds as well as calculating and transmitting to the FC several time-dependent parameters necessary to perform the global detection task.

This architecture is compared with an architecture lacking the PPC and the feedback system where the FC is the highest hierarchical layer. As the FC computes the final decision without temporal aggregation of the local decisions, this solution is here named *Shewhart chart* [30].

2) Two-Layer Fusion Architecture: In this second architecture, the FC collects $\boldsymbol{d}[n_0], \ldots, \boldsymbol{d}[n]$ and directly performs a *Bayesian posterior detection*, therefore incorporating the (temporal-aggregation) functions of the PPC within the FC itself. As a consequence, it becomes the FC's task to provide the estimated position of the faulty item, as well as to transmit updated local thresholds to the respective sensors.

This architecture is compared with an architecture without

feedback system performing an adaptation of the *CUSUM chart* [30].

The architectures employed for executing the Shewhart and CUSUM charts can both be depicted as modifications of the architecture shown in Fig. 2b. In these variations, the feedback channel is absent, and when executing the Shewhart chart, the FC exclusively engages in spatial aggregation.

III. LOCAL DETECTION

This section provides the description of the local detector as it presents the same design strategy among all the presented cases. For the sake of notation, we outline the design for systems with no feedback mechanism (as in the architecture using the Shewhart and CUSUM charts). The changes of notation necessary when using a feedback mechanism are provided at the end of the section.

The edge layer of the proposed architectures consists of the sensors individually taking local decisions. Based on the binary hypothesis in Eq. (10), the optimal test is a *Likelihood Ratio Test* (LRT) on $y_k[n]$, indicated as $\Lambda^k(y_k[n])$. Here, the unknown location of the faulty item is marginalized by employing the stationary prior probability of item failure from Eq. (7). Precisely, for the kth sensor at the nth instant, it holds:

$$\Lambda^k(y_k[n]) \triangleq \frac{p(y_k[n]|\mathcal{H}[n] = 1)}{p(y_k[n]|\mathcal{H}[n] = 0)} \qquad (11)$$

$$= \frac{\displaystyle\sum_{m=1}^{M} \varphi_m\, p(y_k[n]|\mathcal{H}_m[n] = 1)}{p(y_k[n]|\mathcal{H}[n] = 0)}\ .$$

Hence, by leveraging Eq. (10), we get the ML detector:

$$\Lambda^k(y_k[n]) = \sum_{m=1}^{M} \left(\varphi_m\, a_{m,k}\, e^{b_{m,k}\, y_k^2[n]} \right) \underset{d_k[n]=0}{\overset{d_k[n]=1}{\gtrless}} 1\ , \qquad (12)$$

where

$$a_{m,k} \triangleq \sqrt{\frac{\sigma_{w,k}^2}{\sigma_{\xi,m}^2\, g^2(\boldsymbol{x}_k, \boldsymbol{\theta}_m) + \sigma_{w,k}^2}}\ , \qquad (13)$$

$$b_{m,k} \triangleq \frac{1}{2} \left(\frac{1}{\sigma_{w,k}^2} - \frac{1}{\sigma_{\xi,m}^2 \, g^2(\boldsymbol{x}_k, \boldsymbol{\theta}_m) + \sigma_{w,k}^2} \right) . \quad (14)$$

Since $\Lambda^k(y_k[n])$ in Eq. (12) is monotonically increasing with $y_k^2[n]$, there exists a unique value of γ_k such that $\Lambda^k(\sqrt{\gamma_k}) = 1$. Consequently, by the Karlin-Rubin Theorem, the test in Eq. (12) is replaced with the following equivalent energy test [31], which reduces the computational complexity of the local test from $\mathcal{O}(M)$ to $\mathcal{O}(1)$:

$$y_k^2[n] \underset{d_k[n]=0}{\overset{d_k[n]=1}{\gtrless}} \gamma_k . \quad (15)$$

This equals to the determination of the value of γ_k that solves $\Lambda^k(\sqrt{\gamma_k}) = 1$:

$$\sum_{m=1}^{M} \left(\varphi_m \, a_{m,k} \, e^{b_{m,k} \, \gamma_k} \right) = 1 . \quad (16)$$

The left-hand side exhibits smoothness, convexity, and increases with γ_k. Consequently, convergence is assured, starting from any initial value $\gamma_k^{(0)}$ when employing the *Newton-Raphson method* (see [32]):

$$\gamma_k^{(q+1)} = \gamma_k^{(q)} - \frac{\sum_{m=1}^{M} \left(\varphi_m \, a_{m,k} \, e^{b_{m,k} \, \gamma_k^{(q)}} \right) - 1}{\sum_{m=1}^{M} \left(\varphi_m \, a_{m,k} \, b_{m,k} \, e^{b_{m,k} \, \gamma_k^{(q)}} \right)} , \quad (17)$$

where q denotes the iteration index.

We express the theoretical performance of the energy test in Eq. (15), necessary when designing the higher hierarchical layer represented by the FC. Specifically, for the kth sensor, the *probability of detection* $(P_{D,k}^{(m)})$ associated with the failure of the mth item and *probability of false alarm* $(P_{F,k})$ are found from Eq. (10) as in [33]:

$$P_{D,k}^{(m)} \triangleq \mathbb{P}(d_k[n] = 1 | \mathcal{H}_m[n] = 1)$$
$$= \mathbb{P}(y_k^2[n] \geq \gamma_k | \mathcal{H}_m[n] = 1)$$
$$= 2\mathcal{Q} \left(\sqrt{\frac{\gamma_k}{\sigma_{\xi,m}^2 \, g^2(\boldsymbol{x}_k, \boldsymbol{\theta}_m) + \sigma_{w,k}^2}} \right) , \quad (18)$$

$$P_{F,k} \triangleq \mathbb{P}(d_k[n] = 1 | \mathcal{H}[n] = 0) = \mathbb{P}(y_k^2[n] \geq \gamma_k | \mathcal{H}[n] = 0)$$
$$= 2\mathcal{Q} \left(\sqrt{\frac{\gamma_k}{\sigma_{w,k}^2}} \right) . \quad (19)$$

In this section, we used the static prior probabilities of item failure φ_m's obtained using Eq. (7). This causes the local thresholds γ_k's to be time-independent as well. However, our two proposed systems use a feedback system allowing the sensors to be designed using the time-dependent prior probabilities of item failure $\varphi_m[n]$'s calculated via Eq. (6). Its use results in time-dependent values of $\gamma_k[n]$'s (as the values of $\varphi_m[n]$'s are used for its calculation via Eq. (17)), $P_{D,k}^{(m)}[n]$'s, and $P_{F,k}[n]$'s. Thus, the iterative procedure shown in Eq. (17) must be continuously carried out by either the PPC (in the Three-Layer WSN) or the FC (in the Two-Layer WSN), transmitting to the kth sensor the correct value of $\gamma_k[n]$.

There are no energy consumption issues associated with this, as these transmissions are sent by the highest hierarchical layer to the sensors, which only require reception without significant energy expenditure.

IV. STATE OF PRACTICE

This section presents two WSN architectures commonly used for detection purposes and their related localization algorithms: (i) the Shewhart chart where the FC takes per-sample decisions based on the spatial aggregation of the local decisions in that instant; (ii) the CUSUM chart where, instead, the FC aggregates the sensors' decisions in space and time.

Unlike the proposed methods, the baseline architectures shown in this section are not equipped with a feedback mechanism. Moreover, they treat the failure rates λ_m's as deterministic parameters that can be obtained via literature.

A. Shewhart Chart

In this architecture, the optimal test for the FC, at the nth instant, is to perform a LRT on the collected vector $\boldsymbol{d}[n]$ to take a global decision $\widehat{\mathcal{H}}[n]$ [24]:

$$\Lambda^{\mathrm{FC}}(\boldsymbol{d}[n]) \triangleq \frac{\mathbb{P}(\boldsymbol{d}[n] | \mathcal{H}[n] = 1)}{\mathbb{P}(\boldsymbol{d}[n] | \mathcal{H}[n] = 0)}$$
$$= \frac{\sum_{m=1}^{M} \varphi_m \mathbb{P}(\boldsymbol{d}[n] | \mathcal{H}_m[n] = 1)}{\mathbb{P}(\boldsymbol{d}[n] | \mathcal{H}[n] = 0)}$$
$$= \sum_{m=1}^{M} \left(\varphi_m \prod_{k=1}^{K} \ell_{m,k}(d_k[n]) \right) \underset{\widehat{\mathcal{H}}[n]=0}{\overset{\widehat{\mathcal{H}}[n]=1}{\gtrless}} \gamma^* , \quad (20)$$

with γ^* being the decision threshold and $\ell_{m,k}(d_k[n])$ representing the likelihood ratio of a generic local decision $d_k[n]$ with respect to the failure of the mth item:

$$\ell_{m,k}(d_k[n]) \triangleq \frac{\mathbb{P}(d_k[n] | \mathcal{H}_m[n] = 1)}{\mathbb{P}(d_k[n] | \mathcal{H}[n] = 0)}$$
$$= \left(\frac{P_{D,k}^{(m)}}{P_{F,k}} \right)^{d_k[n]} \left(\frac{1 - P_{D,k}^{(m)}}{1 - P_{F,k}} \right)^{1 - d_k[n]} . \quad (21)$$

Similarly, for the FC, it is feasible to calculate the (FC) *probability of detection* $(Q_D^{(m)})$ associated with the failure of the mth item and the *probability of false alarm* (Q_F):[2]

$$Q_D^{(m)} \triangleq \mathbb{P}\left(\widehat{\mathcal{H}}[n] = 1 \middle| \mathcal{H}_m[n] = 1 \right) \quad (22)$$
$$= \sum_{\boldsymbol{d} : \Lambda^{\mathrm{FC}}(\boldsymbol{d}) \geq \gamma^*} \prod_{k=1}^{K} \left[\left(P_{D,k}^{(m)} \right)^{d_k} \left(1 - P_{D,k}^{(m)} \right)^{1 - d_k} \right] ,$$

$$Q_F \triangleq \mathbb{P}\left(\widehat{\mathcal{H}}[n] = 1 \middle| \mathcal{H}[n] = 0 \right) \quad (23)$$
$$= \sum_{\boldsymbol{d} : \Lambda^{\mathrm{FC}}(\boldsymbol{d}) \geq \gamma^*} \prod_{k=1}^{K} \left[(P_{F,k})^{d_k} (1 - P_{F,k})^{1 - d_k} \right] .$$

The derivation of $Q_D^{(m)}$ and Q_F can be found in Appendix B.

We can also express the likelihood ratio at instant n of the decision $\mathcal{D}[n]$ with respect to the mth item, which will be useful in the next sections:

$$\mathcal{L}_m(\mathcal{D}[n]) \triangleq \frac{\mathbb{P}(\mathcal{D}[n] | \mathcal{H}_m[n] = 1)}{\mathbb{P}(\mathcal{D}[n] | \mathcal{H}[n] = 0)}$$

---

[2]The following definitions imply that if $\Lambda^{\mathrm{FC}}(\boldsymbol{d}) = \gamma^*$, then $\widehat{\mathcal{H}}[n] = 1$.

$$= \left(\frac{Q_D^{(m)}}{Q_F}\right)^{\mathcal{D}[n]} \left(\frac{1 - Q_D^{(m)}}{1 - Q_F}\right)^{1 - \mathcal{D}[n]} . \tag{24}$$

It is important to observe that Eqs. (22) and (23) can be precisely computed using a finite number of operations because the number of potential outcomes of $\Lambda^{\mathrm{FC}}(\boldsymbol{d})$ amounts to 2^K. If $\widehat{\mathcal{H}}[n] = 1$, the FC runs a localization algorithm to identify the faulty item. For this algorithm, it is possible to use the following *Maximum A-Posteriori* (MAP) estimator:

$$\widehat{m}[i] = \underset{m=1,\ldots,M}{\arg\max} \left(\varphi_m \prod_{k=1}^{K} \ell_{m,k}(d_k[n])\right), \quad \widehat{\boldsymbol{\theta}}[i] = \boldsymbol{\theta}_{\widehat{m}[i]} , \tag{25}$$

with i indicating the number of times an alarm has been raised, up to instant n.

B. CUSUM Chart

This section describes the CUSUM algorithm to be performed by the FC upon collecting the sensors' local decisions in time.

The CUSUM procedure has the following form:

$$\max_{n_0 \le j \le n} \ln \frac{\mathbb{P}(\boldsymbol{d}[n],\ldots,\boldsymbol{d}[j]|\mathcal{H}[j] = 1)}{\mathbb{P}(\boldsymbol{d}[n],\ldots,\boldsymbol{d}[j]|\mathcal{H}[j] = 0)} \underset{\widehat{\mathcal{H}}[n]=0}{\overset{\widehat{\mathcal{H}}[n]=1}{\gtrless}} \gamma^* . \tag{26}$$

Eq. (26) implicitly estimates the instant corresponding to the system-state change via ML estimation, with the knowledge that the system does not self-repair when in a faulty state. However, Eq. (26) uses the system's state variable $\mathcal{H}[n]$, posing a problem as the only available likelihoods are with respect to the failure of the individual items, and have been explicated in Eq. (18). Due to the finite number of items M, we can use the *Generalized CUSUM* (G-CUSUM) algorithm to address this issue. The following is the G-CUSUM rule:

$$\mathcal{C}[n] \triangleq \max_{n_0 \le j \le n} \ln \frac{\max_m \mathbb{P}(\boldsymbol{d}[n],\ldots,\boldsymbol{d}[j]|\mathcal{H}_m[j] = 1)}{\mathbb{P}(\boldsymbol{d}[n],\ldots,\boldsymbol{d}[j]|\mathcal{H}[j] = 0)}$$

$$= \max_m \max_{n_0 \le j \le n} \ln \frac{\mathbb{P}(\boldsymbol{d}[n],\ldots,\boldsymbol{d}[j]|\mathcal{H}_m[j] = 1)}{\mathbb{P}(\boldsymbol{d}[n],\ldots,\boldsymbol{d}[j]|\mathcal{H}[j] = 0)}$$

$$= \max_m \mathcal{C}_m[n] \underset{\widehat{\mathcal{H}}[n]=0}{\overset{\widehat{\mathcal{H}}[n]=1}{\gtrless}} \gamma^* , \tag{27}$$

which is equivalent to a joint estimation (via ML) of the failure instant and the faulty item. $\mathcal{C}_m[n]$ can be expressed with a *recursive* form starting from its definition and exploiting the independence of the sensor's decision in time:

$$\mathcal{C}_m[n] \triangleq \max_{n_0 \le j \le n} \ln \frac{\mathbb{P}(\boldsymbol{d}[n],\ldots,\boldsymbol{d}[j]|\mathcal{H}_m[j] = 1)}{\mathbb{P}(\boldsymbol{d}[n],\ldots,\boldsymbol{d}[j]|\mathcal{H}[j] = 0)}$$

$$= \max_{n_0 \le j \le n} \sum_{i=j}^{n} \ln \frac{\mathbb{P}(\boldsymbol{d}[i]|\mathcal{H}_m[j] = 1)}{\mathbb{P}(\boldsymbol{d}[i]|\mathcal{H}[j] = 0)} . \tag{28}$$

For $n > n_0$, we can extract the following recursive form:

$$\mathcal{C}_m[n] = \max \left\{ 0, \max_{n_0 \le j \le n-1} \sum_{i=j}^{n-1} \ln \frac{\mathbb{P}(\boldsymbol{d}[i]|\mathcal{H}_m[j] = 1)}{\mathbb{P}(\boldsymbol{d}[i]|\mathcal{H}[j] = 0)} \right\}$$

$$+ \ln \frac{\mathbb{P}(\boldsymbol{d}[n]|\mathcal{H}_m[n] = 1)}{\mathbb{P}(\boldsymbol{d}[n]|\mathcal{H}[n] = 0)}$$

$$= \max\{0, \mathcal{C}_m[n-1]\} + \ln \prod_{k=1}^{K} \ell_{m,k}(d_k[n])$$

$$= (\mathcal{C}_m[n-1])^+ + \sum_{k=1}^{K} \ln \ell_{m,k}(d_k[n]) . \tag{29}$$

On the other hand, when $n = n_0$, by simple application of the definition of $\mathcal{C}_m[n]$, we obtain that $\mathcal{C}_m[n_0] = \sum_{k=1}^{K} \ln \ell_{m,k}(d_k[n_0])$. This results in the following rule:

$$\mathcal{C}_m[n] = \begin{cases} \sum_{k=1}^{K} \ln(\ell_{m,k}(d_k[n_0])), & \text{if } n = n_0 \\ (\mathcal{C}_m[n-1])^+ + \sum_{k=1}^{K} \ln(\ell_{m,k}(d_k[n])), & \text{if } n > n_0 \end{cases} . \tag{30}$$

Also for the case of the CUSUM, if $\widehat{\mathcal{H}}[n] = 1$, a localization procedure is readily available. Such a procedure is the following ML estimator:

$$\widehat{m}[i] = \arg\max_m \mathcal{C}_m[n] , \quad \widehat{\boldsymbol{\theta}}[i] = \boldsymbol{\theta}_{\widehat{m}[i]} , \tag{31}$$

with i indicating the number of times an alarm has been raised, up to instant n.

V. THREE-LAYER FUSION ARCHITECTURE

Here, we present the Three-Layer fusion architecture, which consists of an evolution of the simpler Shewhart chart. In this approach, we add the PPC layer, whose task is to filter the FC's decisions in time using a reliability-based strategy.

A. Fusion Center Detection

In our proposed Three-Layer architecture, the FC, at the nth instant, performs a ML detection, whose task is to fuse the components of $\boldsymbol{d}[n]$ into a single decision $\mathcal{D}[n]$:

$$\Lambda_n^{\mathrm{FC}}(\boldsymbol{d}[n]) \underset{\mathcal{D}[n]=0}{\overset{\mathcal{D}[n]=1}{\gtrless}} 1 , \tag{32}$$

where $\Lambda_n^{\mathrm{FC}}(\boldsymbol{d}[n])$ differs from the statistic in Eq. (20) due to the presence of the feedback system that allows the PPC to transmit parameters to the FC. This feedback allows Eq. (32) to exploit time-dependent parameters such as $\varphi_m[n]$'s, $P_{D,k}^{(m)}[n]$'s, $P_{F,k}[n]$'s, and $\ell_{m,k}^n(d_k[n])$. The values of these parameters are sent to the FC by the PPC.

For this case, the (FC) time-dependent *probability of detection* ($Q_D^{(m)}[n]$) associated with the failure of the mth item and the time-dependent *probability of false alarm* ($Q_F[n]$) at the nth instant can be computed. These are calculated using Eqs. (22) and (23) where the values of $\Lambda^{\mathrm{FC}}(\boldsymbol{d})$, $P_{D,k}^{(m)}$'s, and $P_{F,k}$'s are substituted with those of $\Lambda_n^{\mathrm{FC}}(\boldsymbol{d})$, $P_{D,k}^{(m)}[n]$'s, and $P_{F,k}[n]$'s, respectively. Consequently, the decision likelihood will also be time-dependent (indicated with $\mathcal{L}_m^n(\mathcal{D}[n])$).

B. Post-Processing Center Detection

The primary responsibility of the PPC is to receive $\mathcal{D}[n]$ and determine if an alarm should be triggered. In contrast to local and FC detection, the PPC *incorporates the understanding of the failure model* and utilizes all $\mathcal{D}[j]$ values, where $j = n_0, \ldots, n$, to enact a robust quickest fault detection strategy. For this task, the PPC acts as a Posterior Detector performing a test on $\mathbb{P}(\mathcal{H}[n] = 1|\boldsymbol{\mathcal{D}}[n])$, exploiting Eq. (5) which leads to the following test:

$$\Lambda_n^{\mathrm{PPC}}(\boldsymbol{\mathcal{D}}[n]) \triangleq \sum_{m=1}^{M} \mathbb{P}(\mathcal{H}_m[n] = 1|\boldsymbol{\mathcal{D}}[n])$$
$$= \sum_{m=1}^{M} \mathcal{R}_m^{\mathrm{PPC}}[n] \underset{\widehat{\mathcal{H}}[n]=0}{\overset{\widehat{\mathcal{H}}[n]=1}{\gtrless}} \gamma^* , \qquad (33)$$

where it can be seen that our approach aligns with an *optimal Bayesian perspective* (treating the change point as a random variable whose pdf derives from the reliability model discussed in Sec. II-A). This approach corresponds to the Shiryaev decision rule [30].

The calculation of $\mathcal{R}_m^{\mathrm{PPC}}[n]$ can be expressed recursively via Eq. (34) as shown at the bottom of the page, requiring the storage of only the M values of $\mathcal{R}_m^{\mathrm{PPC}}[n-1]$'s and the value of $\mathcal{D}[n]$, instead of the $(n - n_0 + 1)$ values contained in $\boldsymbol{\mathcal{D}}[n]$. Its derivation is given in Appendix C. Eq. (34) uses $\widehat{\lambda}_m[n]$ since failure rates are considered random variables whose realization must be estimated. The description of this task is given below.

C. Post-Processing Center Localization

When $\widehat{\mathcal{H}}[n] = 1$, the PPC localizes the faulty item for the generic ith time by selecting the index m that maximizes the posterior probability of item failure $\mathcal{R}_m^{\mathrm{PPC}}[n]$ resulting in the following MAP estimator:

$$\widehat{m}[i] = \arg\max_{m} \mathcal{R}_m^{\mathrm{PPC}}[n] , \quad \widehat{\boldsymbol{\theta}}[i] = \boldsymbol{\theta}_{\widehat{m}[i]} , \qquad (35)$$

with i indicating the number of times an alarm has been raised, up to instant n.

D. Post-Processing Center Failure Rate Estimation

The precise failure rate of the unspecified mth item often remains unknown, although literature may frequently offer an estimate (referred to here as $\lambda_{m,0}$) along with its associated variance (referred to as ν_m). Nonetheless, literature data is often derived from a limited number of experiments on items that may not be identical to those within the system (or under the same operating conditions). Consequently, the PPC treats each λ_m as a random variable in this context. This differs from the Shewhart and CUSUM charts that see the failure rates as deterministic parameters and exploit the literature values $\lambda_{m,0}$'s for their calculations.

In specific terms, when the PPC raises an alarm, the system is halted, and an inspection is conducted to assess the system's status. If the mth item's jth failure is confirmed, it becomes feasible to update the estimate of λ_m using $T_{m,j}$. Since $T_{m,j}$ is not directly accessible, the working assumption here is that $T_{m,j} \approx T_{m,j}^*$, a condition met when $\varepsilon_{m,j} \ll \lambda_m^{-1}$ (i.e., when the time delay incurred by the system in detecting the fault is significantly shorter than the mean lifetime of the item).

Utilizing the vector $\boldsymbol{T}_m[j] \triangleq \begin{bmatrix} T_{m,1} & \cdots & T_{m,j} \end{bmatrix}^{\mathrm{T}}$, the PPC calculates the subsequent *Minimum Mean Square Error (MMSE) Estimator* for the mth item:

$$\widehat{\lambda}_{m,j} = \mathbb{E}(\lambda_m|\boldsymbol{T}_m[j]) . \qquad (36)$$

To compute this expectation, the PPC is required to acquire the (posterior) pdf of $\lambda_m|\boldsymbol{T}_m[j]$. Given that $T_{m,j} \sim \mathrm{Exp}(\lambda_m)$, we incorporate previous knowledge about the lifetime of the mth item by modeling $\lambda_m \sim \mathrm{Gamma}(\alpha_{m,0}, \beta_{m,0})$. Here, $\alpha_{m,0} \triangleq (\lambda_{m,0}^2/\nu_m)$ and $\beta_{m,0} \triangleq (\lambda_{m,0}/\nu_m)$ are computed based on existing literature values. We opt for the Gamma distribution because it is the *conjugate prior* of the Exponential distribution (see [34]). Leveraging the use of a conjugate prior, it becomes apparent that $\lambda_m|\boldsymbol{T}_m[j] \sim \mathrm{Gamma}(\alpha_{m,j}, \beta_{m,j})$, with the Gamma parameters calculated *recursively* by the PPC as $\alpha_{m,j} = (\alpha_{m,j-1} + 1)$ and $\beta_{m,j} = (\beta_{m,j-1} + T_{m,j})$. Once the parameters of the (Gamma) posterior pdf of $\lambda_m|\boldsymbol{T}_m[j]$ are determined, the corresponding MMSE estimator following the jth failure is computed using properties of the Gamma distribution:

$$\widehat{\lambda}_{m,j} = \frac{\alpha_{m,j}}{\beta_{m,j}} . \qquad (37)$$

At any given time n, the most recent estimate of λ_m corresponds to $\widehat{\lambda}_{m,\mathcal{S}_m[n-1]}$, where $\mathcal{S}_m[n-1]$ denotes the count of failures for the mth item reported up to time $(n-1)$. For brevity, we will refer to this estimate as $\widehat{\lambda}_m[n]$.

E. Post-Processing Center Parameters Calculation and Transmission

The last step of the PPC at instant n, after updating (if needed) the estimates of the failure rates of the respective items, consists of obtaining the values of $\varphi_m[n+1]$'s via Eq. (6) exploiting $\widehat{\lambda}_m[n+1]$. Next, via Eq. (17), it computes and delivers the values of the local thresholds $\gamma_k[n+1]$'s to the respective sensors to be used for the next local detection.

Once produced the thresholds, the PPC proceeds to calculate the values of $P_{D,k}^{(m)}[n+1]$'s and $P_{F,k}[n+1]$'s via Eqs. (18) and (19) and sends them to the FC alongside the values of $\varphi_m[n+1]$'s. This allows the FC to evaluate $\Lambda_{n+1}^{\mathrm{FC}}(\boldsymbol{d}[n+1])$ via Eq. (20).

In the final step, the PPC computes the values of $Q_D^{(m)}[n+1]$'s and $Q_F[n+1]$ using Eqs. (22) and (23) to be used by the

$$\mathcal{R}_m^{\mathrm{PPC}}[n] \triangleq \mathbb{P}(\mathcal{H}_m[n] = 1|\boldsymbol{\mathcal{D}}[n]) = \begin{cases} \left[1 + \frac{1}{\mathcal{L}_m^{n_0}(\mathcal{D}[n_0])}\left(\frac{1}{1-e^{-\widehat{\lambda}_m[n_0]\Delta t}} - 1\right)\right]^{-1} , & \text{if } n = n_0 \\ \left[1 + \frac{1}{\mathcal{L}_m^n(\mathcal{D}[n])}\left(\frac{1}{1-e^{-\widehat{\lambda}_m[n]\Delta t}(1-\mathcal{R}_m^{\mathrm{PPC}}[n-1])} - 1\right)\right]^{-1} , & \text{if } n > n_0 \end{cases} \qquad (34)$$

PPC itself in the recursive computation of $\Lambda_{n+1}^{\mathrm{PPC}}(\mathcal{D}[n+1])$ via Eqs. (33) and (34).

VI. TWO-LAYER FUSION ARCHITECTURE

This section presents the Two-Layer fusion approach consisting of an evolution of the Three-Layer approach. Here, the FC handles both the spatial and temporal fusion using the same reliability-based strategy as in the PPC. This method is proposed as an improvement of the CUSUM chart introduced in Sec. IV-B. In our proposed Two-Layer architecture, the FC performs three stages of operations that are analogous to those made by the PPC described in Sec. V.

A. Fusion Center Detection

The FC, upon receiving $\boldsymbol{d}[n]$, establishes whether an alarm should be raised. As with the PPC, the FC now utilizes all $\boldsymbol{d}[j]$ values, where $j = n_0, \ldots, n$, to perform a test on $\mathbb{P}(\mathcal{H}[n] = 1 | \boldsymbol{d}[n], \ldots, \boldsymbol{d}[n_0])$:

$$
\begin{aligned}
\Lambda_n^{\mathrm{FC}}(\boldsymbol{d}[n], \ldots, \boldsymbol{d}[n_0]) &\triangleq \sum_{m=1}^{M} \mathbb{P}(\mathcal{H}_m[n] = 1 | \boldsymbol{d}[n], \ldots, \boldsymbol{d}[n_0]) \\
&= \sum_{m=1}^{M} \mathcal{R}_m^{\mathrm{FC}}[n] \underset{\widehat{\mathcal{H}}[n]=0}{\overset{\widehat{\mathcal{H}}[n]=1}{\gtrless}} \gamma^* ,
\end{aligned} \tag{38}
$$

where it is easy to see the similarity with Eq. (33). However, in this case, the FC processes the unfused local decisions.

Also here, $\mathcal{R}_m^{\mathrm{FC}}[n]$ can be expressed recursively via Eq. (39) as shown at the bottom of the page allowing the FC, at the nth instant, to store only the M values of $\mathcal{R}_m^{\mathrm{FC}}[n-1]$'s and the vector $\boldsymbol{d}[n]$. The proof of Eq. (39) is analogous to that given in Appendix C.

B. Fusion Center Localization

Analogously to the Three-Layer architecture, the FC can provide an estimate of the faulty item by maximizing the posterior probability of item failure to raise the ith alarm if $\widehat{\mathcal{H}}[n] = 1$, resulting in the following MAP estimator:

$$
\widehat{m}[i] = \arg\max_m \mathcal{R}_m^{\mathrm{FC}}[n] , \quad \widehat{\boldsymbol{\theta}}[i] = \boldsymbol{\theta}_{\widehat{m}[i]} , \tag{40}
$$

with i indicating the number of times an alarm has been raised, up to instant n.

C. Fusion Center Failure Rate Estimation

As in the Three-Layer architecture, the FC provides an updated estimate of the failure rates λ_m's by treating them as random variables. At each time n, $\widehat{\lambda}_m[n]$ indicates the most recent estimate of λ_m obtained by time $(n-1)$.

TABLE I: Computational complexity of the architectures

Architecture	Layer	Task	Complexity
Shewhart chart	FC	Detection (including localization)	$\mathcal{O}(KM)$
G-CUSUM chart	FC	Detection (including localization)	$\mathcal{O}(KM)$
Three-Layer Fusion Architecture	FC	Detection	$\mathcal{O}(KM)$
	PPC	Detection (incl. loc.)	$\mathcal{O}(M)$
		Failure Rates Update	$\mathcal{O}(1)$ per item
		$\varphi_m[n+1]$'s Calculation	$\mathcal{O}(M)$
		$\gamma_k[n+1]$'s Calculation	$\mathcal{O}(KM)$ per iter.
		$P_{F,k}[n+1]$'s Calculation	$\mathcal{O}(K)$
		$P_{D,k}^{(m)}[n+1]$'s Calculation	$\mathcal{O}(KM)$
		$Q_F[n+1]$ Calculation	$\mathcal{O}(2^K)$
		$Q_D^{(m)}[n+1]$'s Calculation	$\mathcal{O}(2^K M)$
Two-Layer Fusion Architecture	FC	Detection (incl. loc.)	$\mathcal{O}(KM)$
		Failure Rates Update	$\mathcal{O}(1)$ per item
		$\varphi_m[n+1]$'s Calculation	$\mathcal{O}(M)$
		$\gamma_k[n+1]$'s Calculation	$\mathcal{O}(KM)$ per iter.
		$P_{F,k}[n+1]$'s Calculation	$\mathcal{O}(K)$
		$P_{D,k}^{(m)}[n+1]$'s Calculation	$\mathcal{O}(KM)$

D. Fusion Center Parameters Calculation and Transmission

In the final stage of the process, the FC proceeds to update the estimates of the failure rates and subsequently computes the values of $\varphi_m[n+1]$'s using Eq. (6). Following this, it calculates and transmits the values of $\gamma_k[n+1]$'s to the respective sensors for use in the forthcoming energy test, as per Eq. (17).

After obtaining the thresholds, the FC calculates the values of $P_{D,k}^{(m)}[n+1]$'s and $P_{F,k}[n+1]$'s based on Eqs. (18) and (19). These values play a key role in the (recursive) computation of $\Lambda_{n+1}^{\mathrm{FC}}(\boldsymbol{d}[n+1], \ldots, \boldsymbol{d}[n_0])$ using Eqs. (38) and (39).

VII. COMPUTATIONAL COMPLEXITY

This section is focused on the computational complexity of the tasks performed in all the architectures previously outlined.

All the architectures share the same edge-layer design in which each sensor performs an energy test at each discrete instant. Specifically, we were able to lower the computational complexity of the local tests from $\mathcal{O}(M)$ to $\mathcal{O}(1)$, as previously discussed in Sec. III.

Tab. I shows the computational complexity of each architecture with a subdivision by layer (excluding the edge layer) and the task performed. We can notice that the detection techniques relying on the Shewhart and CUSUM charts do not differ in computational complexity thanks to the recursive form of the CUSUM chart shown in Eq. (30). The detection rules used by the FC in both proposed architectures hold the same complexity.

$$
\mathcal{R}_m^{\mathrm{FC}}[n] \triangleq \mathbb{P}(\mathcal{H}_m[n] = 1 | \boldsymbol{d}[n], \ldots, \boldsymbol{d}[n_0]) =
\begin{cases}
\left[1 + \left(\prod_{k=1}^{K} \ell_{m,k}^{n_0}(d_k[n_0]) \right)^{-1} \left(\frac{1}{1 - e^{-\widehat{\lambda}_m[n_0]\Delta t}} - 1 \right) \right]^{-1} , & \text{if } n = n_0 \\[4mm]
\left[1 + \left(\prod_{k=1}^{K} \ell_{m,k}^{n}(d_k[n]) \right)^{-1} \left(\frac{1}{1 - e^{-\widehat{\lambda}_m[n]\Delta t}(1 - \mathcal{R}_m^{\mathrm{FC}}[n-1])} - 1 \right) \right]^{-1} , & \text{if } n > n_0
\end{cases} \tag{39}
$$

An essential difference between the proposed and the baseline architectures is, however, the existence of the feedback system present in the proposed algorithms.

In the Three-Layer architecture, the PPC has a low-complexity detection rule, as this does not perform spatial aggregation of the local decisions. However, the feedback system requires the PPC to obtain the parameters to be transmitted to the sensors and the FC. The calculation of the thresholds $\gamma_k[n+1]$'s is an iterative procedure with a complexity of $\mathcal{O}(KM)$ *per iteration*. Other calculations such as $\varphi_m[n+1]$'s, $\gamma_k[n+1]$'s, $P_{F,k}[n+1]$'s, and $P_{D,k}^{(m)}[n+1]$'s have an overall computational complexity of $\mathcal{O}(KM)$. The highest complexity resides in the calculation of $Q_F[n+1]$'s and $Q_D^{(m)}[n+1]$'s as this is $\mathcal{O}(2^K M)$, making the Three-Layer architecture unsuitable when a high number of sensors is used.

On the other hand, the Two-Layer architecture transfers the spatial aggregation from the PPC to the FC, which now has to perform a spatio-temporal aggregation as well as the task of obtaining the parameters to be transmitted to the sensors. This, although it increases the absolute number of operations, keeps the computational complexity of the operations to be performed by the FC constant at $\mathcal{O}(KM)$, resulting in an overall reduction of complexity thanks to the removal of the operations requiring exponential time.

It is worth noticing that the localization techniques in all four architectures do not require any extra operation and, therefore, do not contribute to an increase in computational complexity. The reason is that such techniques are all based on function maximization via grid search, which has a complexity of $\mathcal{O}(KM)$ (or $\mathcal{O}(M)$ in the Three-Layer architecture). However, such maximization has already been obtained during the detection step. Therefore, in order to complete the localization task, it is simply necessary to store the index generating the highest among the function's values obtained during the detection stage.

VIII. CASE STUDY

A. Simulation Setup

The Goliat FPSO is an offshore oil platform situated in the Norwegian Barents Sea. This platform uses a *subsea production system* composed of various templates placed on the seabed for its operations.[3] The challenging aspect of this setup is that oil leaks occur in deep waters, rendering their detection even more complex. Additionally, due to the significant depths involved, inspections necessitate the use of *remotely operated vehicles* or *autonomous underwater vehicle*, incurring high costs, thus emphasizing the need to minimize false alarms [9]. Simultaneously, offshore operations are subject to stringent environmental regulations, which demand the rapid detection of spills to minimize the dispersion of hydrocarbons [36]. Underwater oil leaks exhibit a distinctive feature in the form of acoustic signals that can be detected using passive acoustic sensors [37], [38]. In this specific setup, each template is equipped with a manifold that is under the surveillance of three passive acoustic sensors. These sensors measure sound pressure

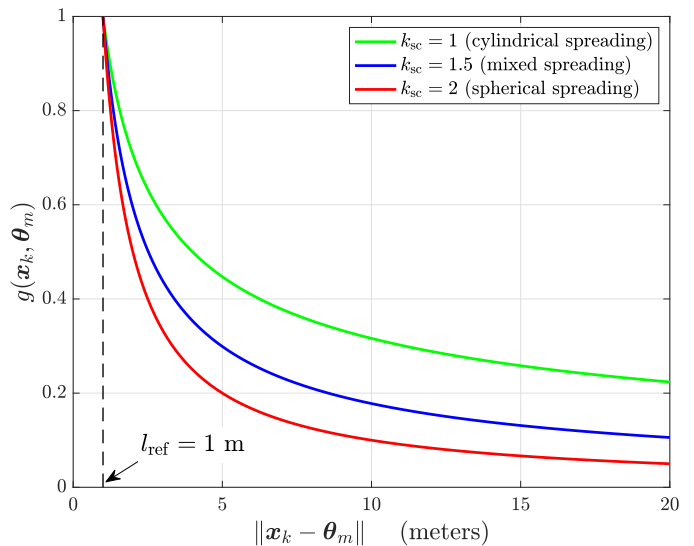[3]For further insights into subsea production systems, please refer to [35]

Fig. 3: Attenuation function vs. distance between sensor and faulty item.

TABLE II: Simulation input parameters

Parameter	Value	Note / Reference
Ref. Frequency	2.5 kHz	[43]
Temperature	3.8 °C	[44]
Salinity	35 ‰	[44]
Depth	350 m	[39]
pH	8	[45]
k_{sc}	1.5	[46]
l_{ref}	1 m	–
Simulated time	15 yr	[47]
Δt	15 min	–
$\sigma_{w,k}^2$	1	$\forall k$
$\mathrm{SNR}_{m,k}$	0/5/10 dB	$\forall\, m, k$

as an integral component of the leak detection system [28], [39].

A reliability analysis recognized $M = 20$ items of interest assumed to be positioned at the same height as the sensors, as shown in Fig. 4. The algorithms described earlier are assumed to have been integrated into the existing system to assess their performance. The attenuation function used is as follows [10]:

$$g(\boldsymbol{x}_k, \boldsymbol{\theta}_m) = \sqrt{\left(\frac{l_{ref}}{\|\boldsymbol{x}_k - \boldsymbol{\theta}_m\|}\right)^{k_{sc}} 10^{(l_{ref} - \|\boldsymbol{x}_k - \boldsymbol{\theta}_m\|)\alpha 10^{-4}}},$$

(41)

where l_{ref} and $\|\boldsymbol{x}_k - \boldsymbol{\theta}_m\|$ are expressed in meters, α is the seawater absorption coefficient in dB/km, and k_{sc} is the dimensionless spreading coefficient. The value of α was determined using the *Francois & Garrison equation* [40], [41]. At the same time, the underwater speed of sound was calculated based on the *Chen & Millero equation* [42], utilizing the input parameters listed in Tab. II. The coefficients of these models are found in [10]. Fig. 3 shows the attenuation of the signal emitted by a faulty item with respect to its distance to a generic sensor using the parameters in Tab. II at varying values of k_{sc}.
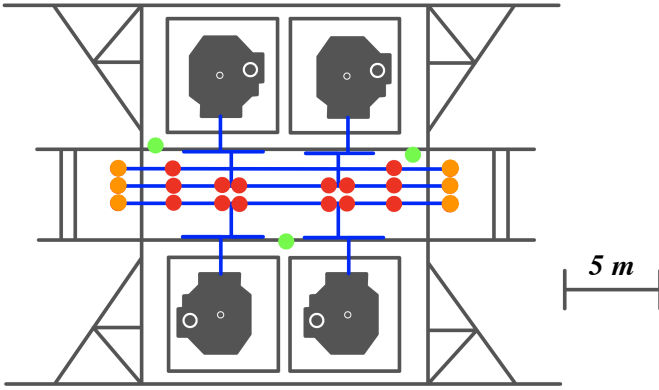
Fig. 4: Goliat's template: the structural components are represented in gray, the manifold in blue, the sensors in green, the valves in red, and the connectors in orange.

TABLE III: Literature failure rates of components in subsea manifolds

Item Category	$\lambda_{m,0}$ (in yr^{-1})	ν_m (in yr^{-2})
Valve, process isolation	7.3000×10^{-3}	7.0715×10^{-5}
Connector	9.5812×10^{-4}	2.4649×10^{-6}

The proposed Three-Layer architecture is compared with the WSN presented in Sec. IV-A. This is because the Three-Layer WSN is designed to be installed over an existing architecture where the final decision is taken by a FC via Shewhart chart by adding a PPC and a feedback system. The Two-Layer architecture is instead compared with the WSN described in Sec. IV-B performing detection via the CUSUM chart. As stated previously, the architectures used for comparison reasons lack a feedback system. The Shewhart and CUSUM charts use the stationary prior probabilities of item failure seen in Eq. (7), where the values of λ_m's are substituted by $\lambda_{m,0}$'s as the former are unknown.

The numerical results were derived via simulation consisting of 200 Monte Carlo runs using Matlab.[4] In these simulations, each run emulated the operational lifespan of the platform, neglecting inspection and maintenance times. The simulated time, the value of Δt, and the diverse $\mathrm{SNR}_{m,k} \triangleq \sigma_{\xi,m}^2/\sigma_{w,k}^2$ values can be found in Tab. II. At each run, a new set of realizations of the M Poisson processes and their corresponding failure rates was generated, with λ_m values drawn from a Gamma distribution using central moments obtained from Tab. III, where literature values were sourced from the *OREDA Handbook* [48].

In order to summarize the main detection results, it is necessary to introduce the following metrics:

$$P_{10} \triangleq \mathbb{P}\Big(\widehat{\mathcal{H}}[n] = 1 \Big| \mathcal{H}[n] = 0\Big) , \qquad (42)$$

$$P_1 \triangleq \mathbb{P}(\mathcal{H}[n] = 1) , \qquad (43)$$

$$\mathrm{ADD} \triangleq \mathbb{E}(\varepsilon_{m,j})/\Delta t , \qquad (44)$$

[4]Each set of 200 runs was performed for various γ^* values to generate the performance curves.

where P_{10} is the *Probability of False Alarm*, P_1 is the *Probability of Faulty State*, and ADD is the *Average Detection Delay*. The localization performances are instead evaluated using the *Root Mean Square Error* (RMSE) between the estimated position of the leak and its actual location. Figs. 5, 6, and 7 show the previously introduced metrics as P_{10} varies in $[10^{-3}, 1]$, at different values of SNR (see Tab. II). Higher values (resp. lower values) of P_{10} can be obtained by decreasing (resp. increasing) the threshold γ^* in the highest architectural layer. The choice of having P_{10} to be on the abscissa in all plots is aimed at improving the readability of the results.
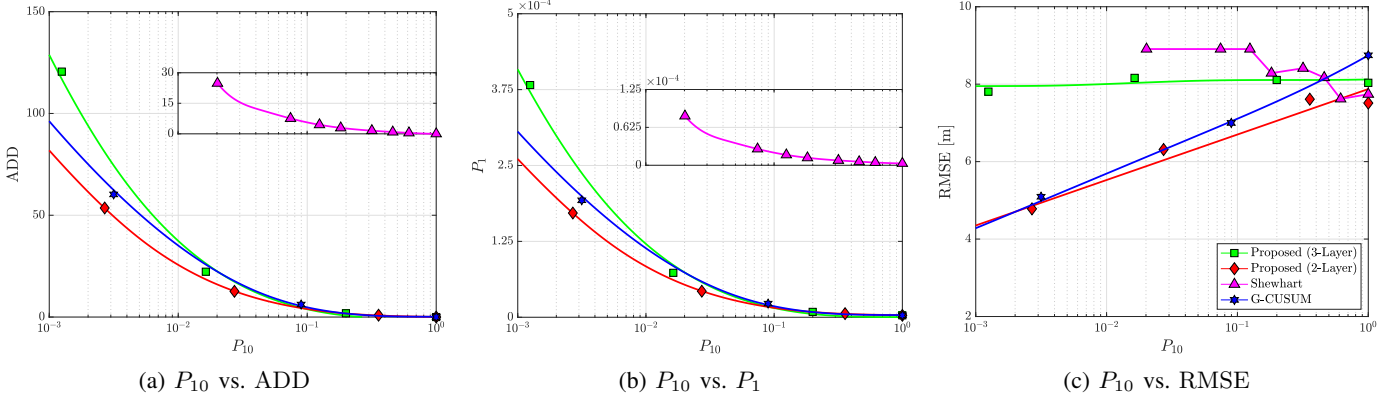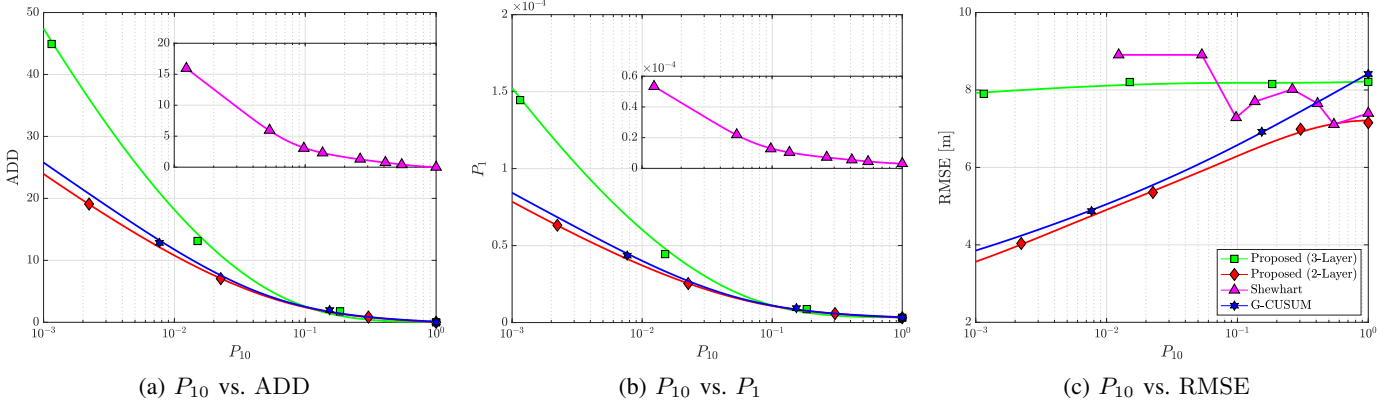
B. Detection Results

By looking at the plots in Figs. 5a, 6a, and 7a, it is immediately visible how ADD greatly decreases as the SNR increases regardless of the employed architecture, once P_{10} is fixed. In particular, the ADD shows a decreasing trend with respect to P_{10} as a consequence of the lowering of threshold γ^*, with ADD $\to 0$ as $P_{10} \to 1$, for all the methods. Specifically, for low values of P_{10}, the proposed Two-Layer architecture shows the lowest values of ADD among the four outlined in this work. It is worth noticing that the Shewhart chart is unable to operate at $P_{10} < 10^{-2}$ due to the lack of temporal integration in the FC. Such a limitation is overcome by using the PPC with our proposed Three-Layer architecture that shows performances equivalent to the Shewhart chart with the further benefit of being able to work at $P_{10} < 10^{-2}$. Moreover, at low SNR, the Three-Layer architecture tends to perform slightly better than the CUSUM chart, highlighting the benefits of a Bayesian approach, especially at low SNR.

These trends in the performances are also observed when evaluating P_1 representing the fraction of time that the system spends in a faulty state. Figs. 5b, 6b, and 7b show a similarity in behavior between the ADD and P_1, as we vary P_{10}. This shows the trade-off between a low P_{10} and a low P_1, which must be addressed when choosing the proper threshold γ^*. As it is desirable to work at low values of P_{10}, it is vital to select an architecture that can limit the effect of having a higher threshold on P_1. Because of the above-mentioned similarities, it is easy to see that, also in this case, the Two-Layer architecture provides the best performances by reaching the lowest values of P_1, given a fixed P_{10}.

It must be mentioned that even in the hypothetical case of $P_{10} = 1$, we will have that $P_1 > 0$ as no architecture can prevent a leak from happening but can only reduce the detection delay with the effect of minimizing P_1.

C. Localization Results

The localization results displayed in Figs. 5c, 6c, and 7c show that, for the case of the Two-Layer proposed architecture and the CUSUM chart, as we lower P_{10}, we simultaneously lower the localization RMSE causing a trade-off between localization accuracy and a quick detection. The explanation for this behavior is that raising the detection threshold has the double effect of increasing the ADD, which simultaneously means that the highest hierarchical layer has collected more inputs, therefore improving the identification of the faulty

(a) P_{10} vs. ADD　　　　(b) P_{10} vs. P_1　　　　(c) P_{10} vs. RMSE
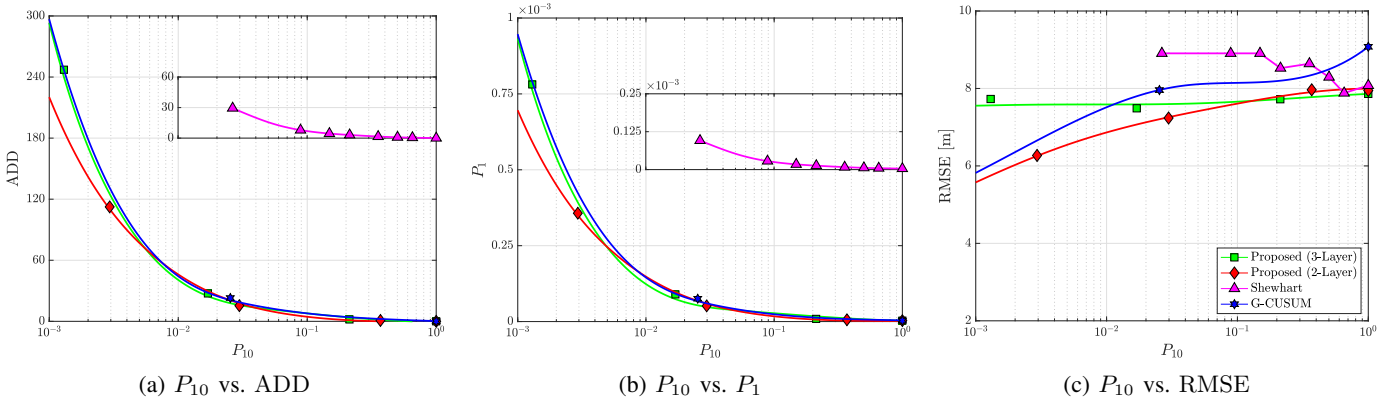
Fig. 5: Performance curves at $\mathrm{SNR}_{m,k} = 0\,\mathrm{dB}$, $\forall m, k$.

(a) P_{10} vs. ADD　　　　(b) P_{10} vs. P_1　　　　(c) P_{10} vs. RMSE

Fig. 6: Performance curves at $\mathrm{SNR}_{m,k} = 5\,\mathrm{dB}$, $\forall m, k$.

(a) P_{10} vs. ADD　　　　(b) P_{10} vs. P_1　　　　(c) P_{10} vs. RMSE

Fig. 7: Performance curves at $\mathrm{SNR}_{m,k} = 10\,\mathrm{dB}$, $\forall m, k$.

item. This does not apply to the Shewhart chart and the Three-Layer architecture: the RMSE observed when employing the Shewhart chart does not have a monotonic behavior (as well as not being able to operate at $P_{10} < 10^{-2}$), while the Three-Layer architecture, as we lower P_{10}, has a virtually null localization improvement.

The behavior associated with the Shewhart chart is given by the nature of its localization algorithm, which produces estimates using only the last vector of local decisions as an input. Such a lack of time aggregation prevents the localization algorithm from updating its estimate as new local decisions are collected over time, which would cause the RMSE to decrease together with P_{10}, like in the case of the Two-Layer architecture and the CUSUM chart. Interestingly, we observe that in the

Shewhart chart, as P_{10} decreases, the behavior of the RMSE is hard to predict. Still, in general, it tends to reach its maximum value when P_{10} reaches its minimum. In fact, for a system performing detection and localization without time aggregation, a trade-off exists between a low P_{10} and localization RMSE. The reason for this is that a lower value of P_{10} means that the threshold required to trigger an alarm must be increased with a consequent effect of triggering alarms only when a higher number of sensors sends a positive detection. However, a low threshold can compromise the ability of the system to localize the faulty item, as there is a loss of correlation between the position of the faulty item and the location of the activated sensors. This can be brought to its limit case of a system detecting a leak via Shewhart chart only when $\Lambda^{\mathrm{FC}}(\boldsymbol{d}[n]) \geq$

γ^*, with $\gamma^* = \Lambda^{\mathrm{FC}}\left(\begin{bmatrix} d_1[n] = 1 & \cdots & d_K[n] = 1 \end{bmatrix}^{\mathrm{T}}\right)$ (i.e., a system that triggers an alarm only when all the sensors send an alarm to the FC). In such a scenario, every alarm would be accompanied by the same localization result regardless of the position of the faulty item.

The Three-Layer architecture, as in the case of the Shewhart chart, does not provide effective results in terms of localization RMSE, confirming its main purpose of being a way to lower the probability of false alarm of the Shewhart chart. Unlike the Shewhart chart, the Three-Layer architecture performs a time aggregation in its highest hierarchical layer (the PPC), creating more stability in the behavior of the localization RMSE, as P_{10} changes. However, such time aggregation is performed on the FC's decisions over time that do not contain any spatial information regarding the sensors that contributed to such decisions. The consequence is an almost constant value of localization RMSE since the system tends to identify as faulty those items that at a generic moment show the highest value of $\widehat{\lambda}_m[n]$, regardless of the spatial location of the activated sensors since this information is unknown for the PPC.

This problem is addressed by the Two-Layer architecture and the CUSUM chart, where the FC performs both time and spatial aggregation of the sensors' local decisions over time. As in the discussion of the detection performances, we notice how the Two-Layer approach outperforms the rest of the architectures in terms of localization RMSE.

D. Final Remarks

In conclusion, the Two-Layer architecture provides the lowest values of ADD, especially at low values of P_{10}, where it guarantees a low P_1, which is a critical goal for Oil and Gas applications. On the other hand, the Three-Layer architecture has proven to be an adequate tool to upgrade an existing network performing the Shewhart chart, especially when low SNR are involved where its detection performances are comparable to those of the CUSUM chart.

As far as the localization task is concerned, it has been observed that the best-performing architectures are those where the highest hierarchical layer performs a spatio-temporal aggregation of the local decisions as in the Two-Layer architecture and the CUSUM chart. Of these two, the Two-Layer architecture is the one able to achieve the lowest RMSE.

It is crucial to emphasize that, on the detection side, the Two-Layer architecture achieves optimality in a Bayesian sense by relying on a posterior detector for decision-making. While the Three-Layer detector also attains Bayesian optimality, it is worth noting that its detection optimality is restricted by the binary nature of the input received by the PPC from the FC. In the proposed methods, the localization procedure can be deemed optimal from a Bayesian perspective, given its reliance on MAP estimation. However, at the system level, localization faces challenges due to detection errors. This is attributed to the fact that the triggering of a localization procedure is conditional to a positive decision, and this decision is based on a rule that does not prioritize the minimization of localization errors, as done in joint detection-localization procedures (see [49], [50]).

The choice of the appropriate detection threshold in the proposed architecture should be obtained via simulation based on a metric to satisfy. Possible strategies for threshold selection include: (a) selecting the threshold corresponding to the maximum value of P_{10} that is tolerated; (b) select a threshold able to guarantee a maximum value of ADD; (c) minimization of P_1; (d) the threshold is chosen using a tailored indicator that takes into consideration all the previous parameters as well as operational factors.

IX. CONCLUSIONS AND FUTURE WORKS

We proposed two architectures addressing the detection and localization task via WSN within industrial plants. Specifically, we proposed a Three-Layer and a Two-Layer Bayesian fusion strategy relying on reliability data for improved performances. In the Three-Layer architecture, we implement a PPC whose task is to perform quickest detection and localization via temporal aggregation of the outputs of a FC that carries out a Shewhart Chart detection rule. Such a temporal aggregation takes advantage of reliability data regarding the monitored system. On the other hand, the Two-Layer architecture directly performs quickest detection and localization at the FC via a spatio-temporal combination of the local decisions taken by the sensors capitalizing on reliability data. Both architectures are equipped with a feedback mechanism necessary for communicating updated parameters from the highest hierarchical layer to the lowest. Two baseline methods, the Shewhart and CUSUM charts, have been introduced. The case study of underwater oil spills in subsea production systems is used to test the proposed architectures, showing the improvements in terms of detection and localization accuracy when the proposed architectures are used. Specifically, the Three-Layer architecture demonstrated the advantages of being able to operate at a lower Probability of False Alarm when compared to the Shewhart chart, which was bound to be higher than 10^{-2}. Meanwhile, the Two-Layer architecture outperforms the CUSUM chart in terms of both detection and localization performance, making it the best-performing architecture among those introduced in the study. In particular, when fixing $P_{10} = 10^{-3}$, the Two-Layer architecture was able to reduce the ADD from around 10% (SNR = 10 dB) up to around 30% (SNR = 0 dB).

Future works include: (a) considering more complex failure models; (b) the reduction of complexity via more efficient techniques for the computation of $Q_D^{(m)}$ and Q_F; (c) modeling erroneous communication channels; (d) a more accurate statistical representation of the signal measured by the sensors, including possible correlations between measured samples in space and time; (e) integration of machine learning strategies for improved detection and localization performances; (f) a study on the distribution of the localization errors; (g) modeling simultaneous faults; (h) development of joint detection and localization techniques.

APPENDIX A
POISSON PROCESS FOR FAILURE MODELING

With the knowledge that $\mathcal{S}_m(t) \sim \mathrm{Poisson}(\lambda_m t)$, we can obtain the failure probability for the mth item $F_m(t)$:

$$F_m(t) = \mathbb{P}(\mathcal{H}_m(t) = 1) = \mathbb{P}\left(T_{m,\mathcal{S}_m(t-\tau_t)+1} \le \tau_t\right)$$

$$= 1 - e^{-\lambda_m \tau_t} \ .$$

We can now obtain $F(t)$. With the knowledge that $\mathcal{H}_m(t) \sim \mathcal{B}(F_m(t))$, we can use the probability-generating function parameterized by z of the variable $\sum_{m=1}^{M} \mathcal{H}_m(t)$:

$$G_{\sum_{m=1}^{M} \mathcal{H}_m(t)}(z) = \prod_{m=1}^{M} G_{\mathcal{H}_m(t)}(z) = \prod_{m=1}^{M} [1 + F_m(t)(z-1)] \ .$$

Using the last result, we can obtain $\mathbb{P}\left(\sum_{m=1}^{M} \mathcal{H}_m(t) = 1\right)$:

$$\mathbb{P}\left(\sum_{m=1}^{M} \mathcal{H}_m(t) = 0\right) = G_{\sum_{m=1}^{M} \mathcal{H}_m(t)}(0) = \prod_{m=1}^{M} (1 - F_m(t)) \ .$$

Thus, we can finally obtain $F(t)$:

$$F(t) = \mathbb{P}(\mathcal{H}(t) = 1) = 1 - \mathbb{P}\left(\sum_{m=1}^{M} \mathcal{H}_m(t) = 0\right)$$

$$= 1 - \prod_{m=1}^{M} (1 - F_m(t)) = 1 - \prod_{m=1}^{M} e^{-\lambda_m \tau_t} \ .$$

However, at low values of $\lambda_m \tau_t$'s, low detection delay, and small Δt, failures behave as disjoint events (*rare events approximation*), therefore:

$$F(t) = \mathbb{P}(\mathcal{H}(t) = 1) \approx \sum_{m=1}^{M} \mathbb{P}(\mathcal{H}_m(t) = 1) = \sum_{m=1}^{M} F_m(t) \ .$$

Thanks to the rare event approximation, we can also retrieve the value of the prior probability of item failure $\varphi_m(t)$:

$$\varphi_m(t) \triangleq \mathbb{P}(\mathcal{H}_m(t) = 1 | \mathcal{H}(t) = 1)$$

$$\approx \frac{\mathbb{P}(\mathcal{H}_m(t) = 1)}{\mathbb{P}(\mathcal{H}(t) = 1)} = \frac{F_m(t)}{F(t)} \ ,$$

Moreover, we can obtain the stationary prior probability of item failure by assuming the failure model as a perfect Poisson process. This is done by calculating the probability that, at a certain time t, the next fault belongs to the mth process:

$$\varphi_m \triangleq \mathbb{P}(\mathcal{H}_m(t) = 1 | \mathcal{H}(t) = 1)$$

$$= \mathbb{P}\left(T_{m,\mathcal{S}_m(t)+1} < T_{f \neq m, \mathcal{S}_{f \neq m}(t)+1}\right) = \frac{\lambda_m}{\sum_{m=1}^{M} \lambda_m} \ .$$

This result is independent of t and $\mathcal{S}_m(t)$.

APPENDIX B
FUSION CENTER PERFORMANCE IN THREE-LAYER WSN

The following is the proof of the performances in Eqs. (22) and (23) of the fusion rule performed by the FC. Regarding the probability of detection associated with the failure of the mth item, we obtain:

$$Q_D^{(m)} \triangleq \mathbb{P}\left(\widehat{\mathcal{H}}[n] = 1 \middle| \mathcal{H}_m[n] = 1\right)$$

$$= \mathbb{P}(\Lambda^{\mathrm{FC}}(\boldsymbol{d}[n]) \geq \gamma^* | \mathcal{H}_m[n] = 1)$$

$$= \sum_{\boldsymbol{d}: \Lambda^{\mathrm{FC}}(\boldsymbol{d}) \geq \gamma^*} \mathbb{P}(\boldsymbol{d} | \mathcal{H}_m[n] = 1)$$

$$= \sum_{\boldsymbol{d}: \Lambda^{\mathrm{FC}}(\boldsymbol{d}) \geq \gamma^*} \prod_{k=1}^{K} \mathbb{P}(d_k | \mathcal{H}_m[n] = 1)$$

$$= \sum_{\boldsymbol{d}: \Lambda^{\mathrm{FC}}(\boldsymbol{d}) \geq \gamma^*} \prod_{k=1}^{K} \left[\left(P_{D,k}^{(m)}\right)^{d_k} \left(1 - P_{D,k}^{(m)}\right)^{1-d_k} \right] \ .$$

The proof exploited the independence of the local decisions. The same steps can be used to prove Q_F.

Note that, in case the WSN is provided with a feedback system (i.e., the time-dependent prior probability of item failure is used), the calculation of the values of $Q_D^{(m)}[n]$'s and $Q_F[n]$ are analogous.

APPENDIX C
RECURSIVE FORM OF PROPOSED DETECTOR

In this appendix, we detail how the expression of $\mathcal{R}_m^{\mathrm{PPC}}[n] \triangleq \mathbb{P}(\mathcal{H}_m[n] = 1 | \boldsymbol{\mathcal{D}}[n])$ can be updated recursively as a function of $\mathcal{R}_m^{\mathrm{PPC}}[n-1]$, for each $m = 1, \ldots, M$ and $n > n_0$.

To begin, we leverage Bayes' Theorem and the conditional independence (i.e., given $\mathcal{H}_m[n]$) of FC decisions $\mathcal{D}[1], \ldots, \mathcal{D}[n]$ over time. By doing this, we get Eq. (45) at the bottom of the next page, in which we further simplified the expression exploiting the following property:

$$\mathbb{P}(\mathcal{D}[n] | \mathcal{H}_m[n], \boldsymbol{\mathcal{D}}[n-1]) = \mathbb{P}(\mathcal{D}[n] | \mathcal{H}_m[n]) \ ,$$

which is a consequence of the uninformativeness of $\boldsymbol{\mathcal{D}}[n-1]$ when inferring $\mathcal{D}[n]$, given that $\mathcal{H}_m[n]$ is known.

Applying the definition of $\mathcal{L}_m^n(\mathcal{D}[n])$, and via algebraic manipulations, we can reformulate Eq. (45) in the following compact form:

$$\mathcal{R}_m^{\mathrm{PPC}}[n] =$$

$$\left[1 + \frac{1}{\mathcal{L}_m^n(\mathcal{D}[n])} \left(\frac{1}{\mathbb{P}(\mathcal{H}_m[n] = 1 | \boldsymbol{\mathcal{D}}[n-1])} - 1 \right) \right]^{-1} \ .$$

Next, we need to obtain $\mathbb{P}(\mathcal{H}_m[n] = 1 | \boldsymbol{\mathcal{D}}[n-1])$. The next set of equations is defined to facilitate the derivation:

$$\mathbb{P}(\mathcal{H}_m[n] | \mathcal{H}_m[n-1], \boldsymbol{\mathcal{D}}[n-1]) = \mathbb{P}(\mathcal{H}_m[n] | \mathcal{H}_m[n-1]), \tag{46}$$

$$\mathbb{P}(\mathcal{H}_m[n] = 1 | \mathcal{H}_m[n-1] = 1) = 1 \ , \tag{47}$$

where Eq. (46) is a consequence of the uninformativeness of $\boldsymbol{\mathcal{D}}[n-1]$ when inferring $\mathcal{H}_m[n]$ given that $\mathcal{H}_m[n-1]$ is known, and Eq. (47) is the impossibility for an item to repair itself.

By applying the Law of Total Probability, we get Eq. (48) at the bottom of next the page. Eq. (48) can be reduced by applying Eq. (46) and (47). Furthermore, exploiting the definition of $\mathcal{R}_m^{\mathrm{PPC}}[n-1]$, Eq. (48) can be written as reported in Eq. (49) at the bottom of the next page.

Moreover, via Eq. (3), it is possible to prove that $\mathcal{H}_m[n] | \mathcal{H}_m[n-1] = 0 \sim \mathcal{B}(1 - e^{-\lambda_m \Delta t})$, leading to Eq. (50) at the bottom of the next page.

Finally, aggregating the previously obtained results, we obtain the recursive expression of $\mathcal{R}_m^{\mathrm{PPC}}[n]$, for $n > n_0$:

$$\mathcal{R}_m^{\mathrm{PPC}}[n] =$$

$$\left[1 + \frac{1}{\mathcal{L}_m^n(\mathcal{D}[n])} \left(\frac{1}{1 - e^{-\lambda_m \Delta t}(1 - \mathcal{R}_m^{\mathrm{PPC}}[n-1])} - 1 \right) \right]^{-1} \ .$$

When $n = n_0$, the problem reduces to $\mathcal{R}_m^{\mathrm{PPC}}[n_0] = \mathbb{P}(\mathcal{H}_m[n_0] = 1|\mathcal{D}[n_0])$. By applying Bayes' Theorem (as we did for the case of $n > n_0$ in Eq. (45)), and knowing that $\mathcal{H}_m[n_0] \sim \mathcal{B}(1 - e^{-\lambda_m \Delta t})$, it becomes easy to prove the following expression:

$$\mathcal{R}_m^{\mathrm{PPC}}[n_0] = \left[1 + \frac{1}{\mathcal{L}_m^{n_0}(\mathcal{D}[n_0])}\left(\frac{1}{1 - e^{-\lambda_m \Delta t}} - 1\right)\right]^{-1}.$$

ACKNOWLEDGMENT

REFERENCES

[1] G. Tabella, D. Ciuonzo, N. Paltrinieri, and P. Salvo Rossi, "Spatio-temporal decision fusion for quickest fault detection within industrial plants: The oil and gas scenario," in *IEEE 24th Int. Conf. Inf. Fusion (FUSION)*, 2021.

[2] J. C. Lopez-Ardao, R. F. Rodriguez-Rubio, A. Suarez-Gonzalez, M. Rodriguez-Perez, and M. E. Sousa-Vieira, "Current trends on green wireless sensor networks," *Sensors*, vol. 21, no. 13, p. 4281, 2021.

[3] K. Rose, S. Eldridge, and L. Chapin, "The Internet of Things: An overview," *The Internet Society (ISOC)*, vol. 80, pp. 1–50, 2015.

[4] S. He, K. Shi, C. Liu, B. Guo, J. Chen, and Z. Shi, "Collaborative sensing in Internet of Things: A comprehensive survey," *IEEE Commun. Surveys Tuts.*, vol. 24, no. 3, pp. 1435–1474, 2022.

[5] T. Sahoo, *Process Plants - Shutdown and Turnaround Management*. Boca Raton (FL), USA: Taylor & Francis Group, 2014.

[6] Market Research Future, "Market Research Report," 2023.

[7] N. Paltrinieri, G. Landucci, and P. Salvo Rossi, "Real-Time Data for Risk Assessment in the Offshore Oil and Gas Industry," in *Int. Conf. Offshore Mech. Arct. Eng. (OMAE)*, 2017.

[8] Y. Song, "Underwater Acoustic Sensor Networks With Cost Efficiency for Internet of Underwater Things," *IEEE Trans. Ind. Electron.*, vol. 68, no. 2, pp. 1707–1716, 2021.

[9] C. Mai, S. Pedersen, L. Hansen, K. L. Jepsen, and Z. Yang, "Subsea infrastructure inspection: A review study," in *IEEE Int. Conf. Underw. Syst. Technol.: Theory Appl. (USYS)*, 2016, pp. 71–76.

[10] G. Tabella, N. Paltrinieri, V. Cozzani, and P. Salvo Rossi, "Wireless sensor networks for detection and localization of subsea oil leakages," *IEEE Sens. J.*, vol. 21, no. 9, pp. 10 890–10 904, 2021.

[11] M. A. Al-Jarrah, M. A. Yaseen, A. Al-Dweik, O. Dobre, and E. Alsusa, "Decision fusion for IoT-based wireless sensor networks," *IEEE Internet Things J.*, vol. 7, no. 2, pp. 1313–1326, 2019.

[12] D. Ciuonzo, P. Salvo Rossi, and P. K. Varshney, "Distributed detection in wireless sensor networks under multiplicative fading via generalized score tests," *IEEE Internet Things J.*, vol. 8, no. 11, pp. 9059–9071, 2021.

[13] N. Paltrinieri, F. Khan, P. Amyotte, and V. Cozzani, "Dynamic approach to risk management: Application to the Hoeganaes metal dust accidents," *Process Saf. Environ. Protect.*, vol. 92, no. 6, pp. 669–679, 2014.

[14] V. Villa, N. Paltrinieri, F. Khan, and V. Cozzani, "Towards dynamic risk analysis: A review of the risk assessment approach and its limitations in the chemical process industry," *Saf. Sci.*, vol. 89, pp. 77–93, 2016.

[15] T. Grøtan and N. Paltrinieri, "Dynamic risk management in the perspective of a resilient system," in *Dynamic Risk Analysis in the Chemical and Petroleum Industry*. Elsevier, 2016, pp. 245–257.

[16] N. Paltrinieri, L. Comfort, and G. Reniers, "Learning about risk: Machine learning for risk assessment," *Saf. Sci.*, vol. 118, pp. 475–486, 2019.

[17] R. Niu and P. K. Varshney, "Performance analysis of distributed detection in a random sensor field," *IEEE Trans. Signal Process.*, vol. 56, no. 1, pp. 339–349, 2007.

[18] S. Sen, N. S. V. Rao, C. Q. Wu, M. L. Berry, K. M. Grieme, R. R. Brooks, and G. Cordone, "Performance analysis of Wald-statistic based network detection methods for radiation sources," in *19th Int. Conf. Inf. Fusion (FUSION)*, 2016, pp. 820–827.

[19] N. Sriranga, K. G. Nagananda, R. S. Blum, A. Saucan, and P. K. Varshney, "Energy-efficient decision fusion for distributed detection in wireless sensor networks," in *21th Int. Conf. Inf. Fusion (FUSION)*, 2018, pp. 1541–1547.

[20] G. Tabella, N. Paltrinieri, V. Cozzani, and P. Salvo Rossi, "Subsea oil spill risk management based on sensor networks," *Chem. Eng. Trans.*, vol. 82, pp. 199–204, 2020.

[21] M. Bucelli, I. B. Utne, P. Salvo Rossi, and N. Paltrinieri, "A system engineering approach to subsea spill risk management," *Saf. Sci.*, vol. 123, 2020.

[22] G. Tabella, N. Paltrinieri, V. Cozzani, and P. Salvo Rossi, "Data fusion for subsea oil spill detection through wireless sensor networks," in *Proc. IEEE Sensors*, 2020.

[23] A. Shoari and A. Seyedi, "Detection of a non-cooperative transmitter in Rayleigh fading with binary observations," in *IEEE Mil. Commun. Conf. (MILCOM)*, 2012, pp. 1–5.

[24] D. Ciuonzo and P. Salvo Rossi, "Distributed detection of a non-cooperative target via generalized locally-optimum approaches," *Inf. Fusion*, vol. 36, pp. 261–274, 2017.

[25] L. Hu, J. Zhang, X. Wang, S. Wang, and E. Zhang, "Decentralized truncated one-sided sequential detection of a noncooperative moving target," *IEEE Signal Process. Lett.*, vol. 25, no. 10, pp. 1490–1494, 2018.

[26] X. Cheng, D. Ciuonzo, P. Salvo Rossi, X. Wang, and W. Wang, "Multi-bit & sequential decentralized detection of a noncooperative moving target through a generalized Rao test," *IEEE Trans. Signal Inf. Process. Netw.*, vol. 7, pp. 740–753, 2021.

[27] J. Pan and J. McElhannon, "Future edge cloud and edge computing for internet of things applications," *IEEE Internet Things J.*, vol. 5, no. 1, pp. 439–449, 2017.

[28] E. Røsby, "Goliat development project - Subsea leak detection design," Aker Solutions, 2011.

[29] M. Rausand and A. Høyland, *System reliability theory: models, statistical methods, and applications*, 2nd ed., ser. (Wiley series in probability and statistics). Hoboken (NJ), USA: Wiley-Interscience, 2004.

[30] L. Xie, S. Zou, Y. Xie, and V. V. Veeravalli, "Sequential (quickest) change detection: Classical results and new directions," *IEEE J. Sel. Areas Inf. Theory*, vol. 2, no. 2, pp. 494–514, 2021.

[31] G. Casella and R. L. Berger, *Statistical Inference*, 2nd ed. Pacific Grove (CA), USA: Thomson Learning, 2002.

[32] D. Kincaid and W. Cheney, *Numerical Analysis: Mathematics of Scientific Computing*, 3rd ed. Providence (RI), USA: American Mathematical Society, 2002.

[33] S. Kay, *Fundamentals of Statistical Signal Processing: Detection Theory*, ser. (Prentice Hall Signal Processing Series). Upper Saddle River (NJ), USA: Prentice-Hall, 1998.

[34] M. Rausand and S. Haugen, *Risk Assessment: Theory, Methods, and Applications*, 1st ed. Hoboken (NJ), USA: John Wiley & Sons, 2011.

$$\mathcal{R}_m^{\mathrm{PPC}}[n] = \frac{\mathbb{P}(\mathcal{D}[n]|\mathcal{H}_m[n] = 1)\mathbb{P}(\mathcal{H}_m[n] = 1|\boldsymbol{\mathcal{D}}[n-1])}{\mathbb{P}(\mathcal{D}[n]|\mathcal{H}_m[n] = 1)\mathbb{P}(\mathcal{H}_m[n] = 1|\boldsymbol{\mathcal{D}}[n-1]) + \mathbb{P}(\mathcal{D}[n]|\mathcal{H}_m[n] = 0)[1 - \mathbb{P}(\mathcal{H}_m[n] = 1|\boldsymbol{\mathcal{D}}[n-1])]} \tag{45}$$

$$\mathbb{P}(\mathcal{H}_m[n] = 1|\boldsymbol{\mathcal{D}}[n-1]) = \sum_{i=0}^{1} \mathbb{P}(\mathcal{H}_m[n] = 1|\boldsymbol{\mathcal{D}}[n-1], \mathcal{H}_m[n-1] = i)\mathbb{P}(\mathcal{H}_m[n-1] = i) \tag{48}$$

$$\mathbb{P}(\mathcal{H}_m[n] = 1|\boldsymbol{\mathcal{D}}[n-1]) = 1 - [1 - \mathbb{P}(\mathcal{H}_m[n] = 1|\mathcal{H}_m[n-1] = 0)](1 - \mathcal{R}_m^{\mathrm{PPC}}[n-1]) \tag{49}$$

$$\mathbb{P}(\mathcal{H}_m[n] = 1|\boldsymbol{\mathcal{D}}[n-1]) = 1 - e^{-\lambda_m \Delta t}(1 - \mathcal{R}_m^{\mathrm{PPC}}[n-1]) \tag{50}$$

[35] Y. Bai and Q. Bai, *Subsea Engineering Handbook*. Houston (TX), USA: Elsevier, 2012.

[36] DNV-GL, "Recommended practice RP-F302 offshore leak detection," Oslo, Norway, 2016.

[37] H. V. Fuchs and R. Riehle, "Ten years of experience with leak detection by acoustic signal analysis," *Appl. Acoust.*, vol. 33, no. 1, pp. 1–19, 1991.

[38] M. A. Adegboye, W. K. Fung, and A. Karnik, "Recent advances in pipeline monitoring and oil leakage detection technologies: Principles and approaches," *Sensors*, vol. 19, no. 11, p. 2548, 2019.

[39] E. Bjørnbom, "Goliat – Leak detection and monitoring from template to satellite," 2011.

[40] R. E. Francois and G. R. Garrison, "Sound absorption based on ocean measurements: Part I: Pure water and magnesium sulfate contributions," *J. Acoust. Soc. Am.*, vol. 72, no. 3, pp. 896–907, 1982.

[41] ——, "Sound absorption based on ocean measurements: Part II: Boric acid contribution and equation for total absorption," *J. Acoust. Soc. Am.*, vol. 72, no. 6, pp. 1879–1890, 1982.

[42] G. S. K. Wong and S. Zhu, "Speed of sound in seawater as a function of salinity, temperature, and pressure," *J. Acoust. Soc. Am.*, vol. 97, no. 3, pp. 1732–1736, 1995.

[43] E. G. Eckert, J. W. Maresca, R. W. Hillger, and J. J. Yezzi, "Location of leaks in pressurized petroleum pipelines by means of passive-acoustic sensing methods," in *Leak Detection for Underground Storage Tanks*. West Conshohocken (PA), USA: ASTM Int., 1993, pp. 53–69.

[44] Institute of Marine Research, "Mareano," 2021.

[45] A. A. Vetrov and E. A. Romankevich, *Carbon Cycle in the Russian Arctic Seas*. Berlin, Germany: Springer, 2004.

[46] M. Stojanovic, "On the relationship between capacity and distance in an underwater acoustic communication channel," in *Int. Workshop Underw. Netw. (WUWNet)*, 2006, pp. 34–43.

[47] Vår Energi, "Goliat Barrier Status Panel," 2016.

[48] SINTEF, *OREDA Offshore Reliability Data Handbook*, 4th ed. OREDA Participants, 2002.

[49] A. Tajer, G. H. Jajamovich, X. Wang, and G. V. Moustakides, "Optimal joint target detection and parameter estimation by mimo radar," *IEEE J. Sel. Top. Signal Process.*, vol. 4, no. 1, pp. 127–145, 2010.

[50] G. V. Moustakides, G. H. Jajamovich, A. Tajer, and X. Wang, "Joint detection and estimation: Optimum tests and applications," *IEEE Trans. Inf. Theory*, vol. 58, no. 7, pp. 4215–4229, 2012.

Domenico Ciuonzo (Senior Member, IEEE) received the Ph.D. degree in Electronic Engineering from the University of Campania, Italy, in 2013. He is an Assistant Professor with the University of Naples "Federico II", Naples, Italy. Since 2011, he has been holding several visiting researcher appointments. His research interests include data fusion, wireless sensor networks, the Internet of Things, and machine learning. Dr. Ciuonzo is a recipient of Best Paper Awards from the IEEE International Conference on Computer and Communication Systems in 2019 and Computer Networks in 2020, the Exceptional Service Award from IEEE Aerospace and Electronic Systems Society in 2019, and the Early-Career Technical Achievement Award from IEEE Sensors Council of sensor networks/systems in 2020. Since 2014, he has been an (Area) Editor of several IEEE journals.

Nicola Paltrinieri received the B.Sc. degree in chemical engineering, the M.Sc. degree (*summa cum laude*) in chemical and process engineering and the Ph.D. degree in environmental, safety and chemical engineering from the University of Bologna, Italy, in 2005, 2008 and 2012, respectively. From 2012 to 2016, he was Research Scientist at the Dept. Safety Research, SINTEF Technology and Society (Norway), and in 2012 he held a postdoctoral position at the University of Bologna. He has been a Professor of risk analysis at the Norwegian University of Science and Technology (NTNU), Norway, and an Adjunct Professor of offshore HSE management at the University of Bologna, Italy, since 2016. His research focuses on both the method and the application of risk analysis within socio-technical systems. Regarding the former, he has investigated the concepts and techniques supporting dynamic risk analysis, from uncertainty to machine learning. Regarding the latter, he has worked on risk analysis for safety-critical emerging technologies (e.g., hydrogen technologies). Prof. Paltrinieri is a chartered engineer in the British Engineering Council register, and a charted scientist in the British Science Council register. He is a member of the editorial boards of the journal SAFETY SCIENCE, JOURNAL OF MARINE SCIENCE AND ENGINEERING, JOURNAL OF RISK RESEARCH, and SAFETY IN EXTREME ENVIRONMENTS. He is the leader of NTNU Energy Team Hydrogen. He serves as Norwegian delegate of the Working Party on Loss Prevention and Safety Promotion within the European Federation of Chemical Engineering. He is co-chair of Accident and Incident Modeling, European Safety and Reliability Association Technical Committee. He has served as a member of the scientific committees for the ESREL, Loss Prevention, and CISAP conferences since 2016.

Pierluigi Salvo Rossi (Senior Member, IEEE) was born in Naples, Italy, in 1977. He received the Dr.Eng. degree (*summa cum laude*) in telecommunications engineering and the Ph.D. degree in computer engineering from the University of Naples "Federico II", Italy, in 2002 and 2005, respectively. He is a Full Professor and the Deputy Head with the Department of Electronic Systems, Norwegian University of Science and Technology (NTNU), Trondheim, Norway. He is also a part-time Research Scientist with the Department of Gas Technology, SINTEF Energy Research, Norway.

Previously, he worked with the University of Naples "Federico II", Italy, with the Second University of Naples, Italy, with NTNU, Norway, and with Kongsberg Digital AS, Norway. He held visiting appointments with Drexel University, USA, Lund University, Sweden, NTNU, Norway, and Uppsala University, Sweden. His research interests fall within communication theory, data fusion, machine learning, and signal processing.

Prof. Salvo Rossi was awarded as an Exemplary Senior Editor of the IEEE COMMUNICATIONS LETTERS in 2018. He is (or has been) on the Editorial Board of the IEEE OPEN JOURNAL OF THE COMMUNICATIONS SOCIETY, the IEEE TRANSACTIONS ON SIGNAL AND INFORMATION PROCESSING OVER NETWORKS, the IEEE SENSORS JOURNAL, the IEEE COMMUNICATIONS LETTERS, and the IEEE TRANSACTIONS ON WIRELESS COMMUNICATIONS.

Gianluca Tabella (Graduate Student Member, IEEE) was born in Suzzara, Italy, in 1993. He received the B.Sc. degree in chemical and biochemical engineering (curriculum process engineering) and the M.Sc. degree in chemical and process engineering (curriculum offshore engineering) from the University of Bologna, Italy, in 2017 and 2019, respectively. Since 2020, he has been working towards the Ph.D. degree in electronics and telecommunication at the Dept. Electronic Systems, Norwegian University of Science and Technology (NTNU), Trondheim, Norway. He is a Research Scientist at the Dept. Gas Technology, SINTEF Energy Research, Trondheim, Norway. In 2022, he was a visiting scholar at the Dept. Electrical Engineering, Columbia University, New York (NY), USA. His research interests are in distributed detection and localization, focusing on the process and energy industries.